Title: Modified Gravity and its Consequences for the Solar System, Astrophysics and Cosmology

Date: May 20, 2007 04:30 PM

URL: http://pirsa.org/07050045

Abstract: A relativistic modified gravity (MOG) leads to a self-consistent, stable gravity theory that can describe the solar system, galaxy and clusters of galaxies data and cosmology without dark matter. A review is given of fits to galaxy rotation curves, mass profiles of X-ray clusters and weak and strong lensing of galaxy clusters including the bullet cluster E10657-56. MOG can explain the CMB power spectrum and the observed acceleration of the expansion of the universe.

Modified Gravity And Its Consequences For The Solar System, Astrophysics And Cosmology

J. W. Moffat

Perimeter Institute For Theoretical Physics,

Waterloo, Ontario, Canada

Talk given at the Workshop "Excursions in the Dark", Perimeter Institute, May 18 -20, 2007

Modified Gravity And Its Consequences For The Solar System, Astrophysics And Cosmology

J. W. Moffat

Perimeter Institute For Theoretical Physics,

Waterloo, Ontario, Canada

Talk given at the Workshop "Excursions in the Dark", Perimeter Institute, May 18 -20, 2007

Contents

1. Introduction

Ingredients of the standard cosmology:

- General Relativity
- Large-scale homogeneity and isotropy
- 5% ordinary matter (baryons and electrons)
- 25% dark matter
- 70% dark energy
- Uniform CMB radiation, T ~ 2.73 degrees
- Scale-free adiabatic fluctuations $\Delta T/T \sim 10^{-5}$

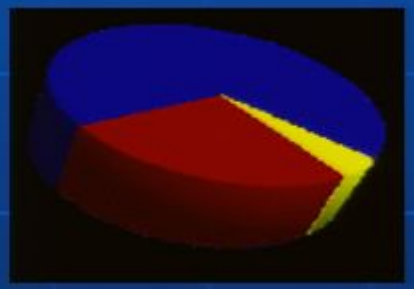

• The dark matter and dark energy are the most puzzling parts of the standard cosmology.

Dark matter is cold and collisionless, ~ 25 %

Dark energy ~ 70 % is smooth and appears about 9 billion years after the Big Bang (supernovae measurements)

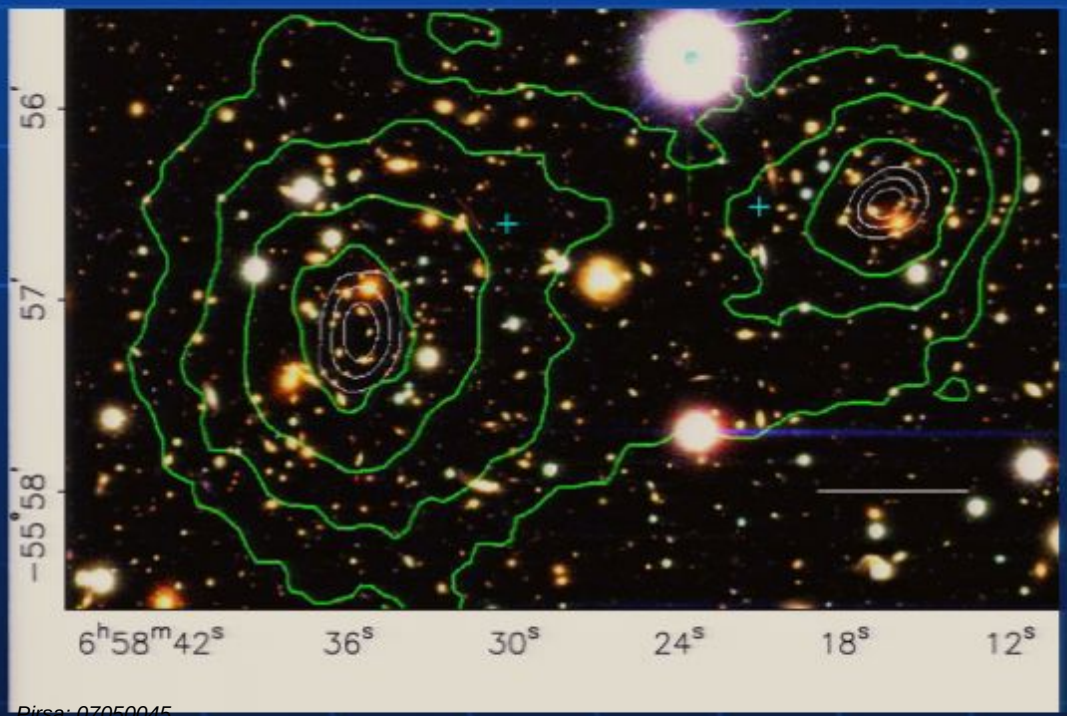

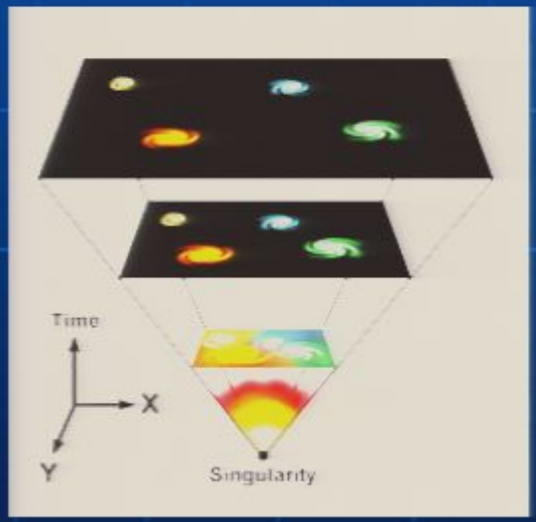

- Dark matter and dark energy are inferred from the motions of visible matter in a gravitational field. It is possible that dark matter doesn't exist and that Einstein's General Relativity (GR) has to be modified. Is this possible? Yes.

- The Equivalence Principle implies a metric and GR is determined uniquely in a 4-dimensional spacetime. To modify GR we either change the Einstein-Hilbert action, pseudo-Riemannian geometry or add new fields.

- The new fields may be dynamically sourced by ordinary matter (baryonic matter) – "modified gravity" (MOG).

• A fully relativistic modified gravity (MOG) called Metric-Skew-Tensor-Gravity (NGT, MSTG) (JWM, 1995, 2005) or Scalar-Tensor-Vector-Gravity (STVG) (JWM, 2006) leads to a self-consistent, stable gravity theory that can describe solar system, astrophysical and cosmological data. The STVG theory has an extra degree of freedom, a vector field called a "phion" field whose curl is a skew field that couples to matter ("fifth force"). The gravitational field is described by a symmetric Einstein metric tensor.

- A fully relativistic modified gravity (MOG) called Metric-Skew-Tensor-Gravity (NGT, MSTG) (JWM, 1995, 2005) or Scalar-Tensor-Vector-Gravity (STVG) (JWM, 2006) leads to a self-consistent, stable gravity theory that can describe solar system, astrophysical and cosmological data. The STVG theory has an extra degree of freedom, a vector field called a "phion" field whose curl is a skew field that couples to matter ("fifth force"). The gravitational field is described by a symmetric Einstein metric tensor.

- The effective classical theory allows the gravitational coupling "constant" G to vary as a scalar field with space and time. The effective mass of the skew symmetric field and the coupling of the field to matter also vary with space and time as scalar fields.

- A fully relativistic modified gravity (MOG) called Metric-Skew-Tensor-Gravity (NGT, MSTG) (JWM, 1995, 2005) or Scalar-Tensor-Vector-Gravity (STVG) (JWM, 2006) leads to a self-consistent, stable gravity theory that can describe solar system, astrophysical and cosmological data. The STVG theory has an extra degree of freedom, a vector field called a "phion" field whose curl is a skew field that couples to matter ("fifth force"). The gravitational field is described by a symmetric Einstein metric tensor.
- The effective classical theory allows the gravitational coupling "constant" G to vary as a scalar field with space and time. The effective mass of the skew symmetric field and the coupling of the field to matter also vary with space and time as scalar fields.
- The variation of the constants can be explained in a quantum gravity renormalization group (RG) flow scenario in which gravity is an asymptotically-free theory (Reuter and Weyer, JWM, 2005).

• The modified Newtonian acceleration law for weak fields can fit a large amount of galaxy rotation curve data without non-baryonic dark matter (J.R.Brownstein and JWM, 2006). It also can fit data for X-ray galaxy clusters without dark matter. The modified acceleration law is consistent with the solar system data and can possibly explain the Pioneer 10-11 anomalous acceleration (J. R. Brownstein & JWM, 2006, JWM 2006).

- The modified Newtonian acceleration law for weak fields can fit a large amount of galaxy rotation curve data without non-baryonic dark matter (J.R.Brownstein and JWM, 2006). It also can fit data for X-ray galaxy clusters without dark matter. The modified acceleration law is consistent with the solar system data and can possibly explain the Pioneer 10-11 anomalous acceleration (J. R. Brownstein & JWM, 2006, JWM 2006).

The MOG must also explain the following:

- The CMB data including the power spectrum data;

• The modified Newtonian acceleration law for weak fields can fit a large amount of galaxy rotation curve data without non-baryonic dark matter (J.R.Brownstein and JWM, 2006). It also can fit data for X-ray galaxy clusters without dark matter. The modified acceleration law is consistent with the solar system data and can possibly explain the Pioneer 10-11 anomalous acceleration (J. R. Brownstein & JWM, 2006, JWM 2006).

The MOG must also explain the following:

• The CMB data including the power spectrum data;

• The formation of proto-galaxies in the early universe and the growth of galaxies;

• The modified Newtonian acceleration law for weak fields can fit a large amount of galaxy rotation curve data without non-baryonic dark matter (J.R.Brownstein and JWM, 2006). It also can fit data for X-ray galaxy clusters without dark matter. The modified acceleration law is consistent with the solar system data and can possibly explain the Pioneer 10-11 anomalous acceleration (J. R. Brownstein & JWM, 2006, JWM 2006).

The MOG must also explain the following:

• The CMB data including the power spectrum data;

• The formation of proto-galaxies in the early universe and the growth of galaxies;

• Gravitational lensing data for galaxies and clusters of galaxies;

• The modified Newtonian acceleration law for weak fields can fit a large amount of galaxy rotation curve data without non-baryonic dark matter (J.R.Brownstein and JWM, 2006). It also can fit data for X-ray galaxy clusters without dark matter. The modified acceleration law is consistent with the solar system data and can possibly explain the Pioneer 10-11 anomalous acceleration (J. R. Brownstein & JWM, 2006, JWM 2006).

The MOG must also explain the following:

• The CMB data including the power spectrum data;

• The formation of proto-galaxies in the early universe and the growth of galaxies;

• Gravitational lensing data for galaxies and clusters of galaxies;

• The Bullet Cluster 1E0-657-56;

• N-body simulations of galaxy surveys;

• The modified Newtonian acceleration law for weak fields can fit a large amount of galaxy rotation curve data without non-baryonic dark matter (J.R.Brownstein and JWM, 2006). It also can fit data for X-ray galaxy clusters without dark matter. The modified acceleration law is consistent with the solar system data and can possibly explain the Pioneer 10-11 anomalous acceleration (J. R. Brownstein & JWM, 2006, JWM 2006).

The MOG must also explain the following:

• The CMB data including the power spectrum data;

• The formation of proto-galaxies in the early universe and the growth of galaxies;

• Gravitational lensing data for galaxies and clusters of galaxies;

• The Bullet Cluster 1E0-657-56;

• N-body simulations of galaxy surveys;

• The accelerating expansion of the universe.

2. Modified Gravity (MOG)

Our STVG action takes the form $S = S_{\rm Grav} + S_\phi + S_S + S_M$

$$S_{\rm Grav} = \frac{1}{16\pi}\int d^4x\sqrt{-g}\left[\frac{1}{G}(R+2\Lambda)\right],$$

$$S_\phi = -\int d^4x\sqrt{-g}\left[\omega\left(\frac{1}{4}B^{\mu\nu}B_{\mu\nu}+V(\phi)\right)\right],$$

$$S_S = \int d^4x\sqrt{-g}\left[\frac{1}{G^3}\left(\frac{1}{2}g^{\mu\nu}\nabla_\mu G\nabla_\nu G - V(G)\right)\right.$$

$$\left.+\frac{1}{G}\left(\frac{1}{2}g^{\mu\nu}\nabla_\mu\omega\nabla_\nu\omega - V(\omega)\right)+\frac{1}{\mu^2 G}\left(\frac{1}{2}g^{\mu\nu}\nabla_\mu\mu\nabla_\nu\mu - V(\mu)\right)\right]$$

- Metric $g_{\mu\nu}(x)$, massive vector field $\phi_\mu(x)$, 3 scalar fields $G(x)$, $\omega(x)$ and $\mu(x)$.

The modified weak field acceleration law is given by

$$a(r) = -\frac{G(r)M}{r^2}$$

$$G(r) = G_0\left[1+\alpha(r)\left(1-\exp(-r/\lambda(r))\left(1+\frac{r}{\lambda(r)}\right)\right)\right]$$

Renormalization group (RG) flow "running" of $\alpha(r) = (M_0(r)/M)^{1/2} = f(\delta(r)/\mu_\alpha)$ and $\lambda(r) = 1/r_0(r) = h(\zeta(r)/\mu_\lambda)$.

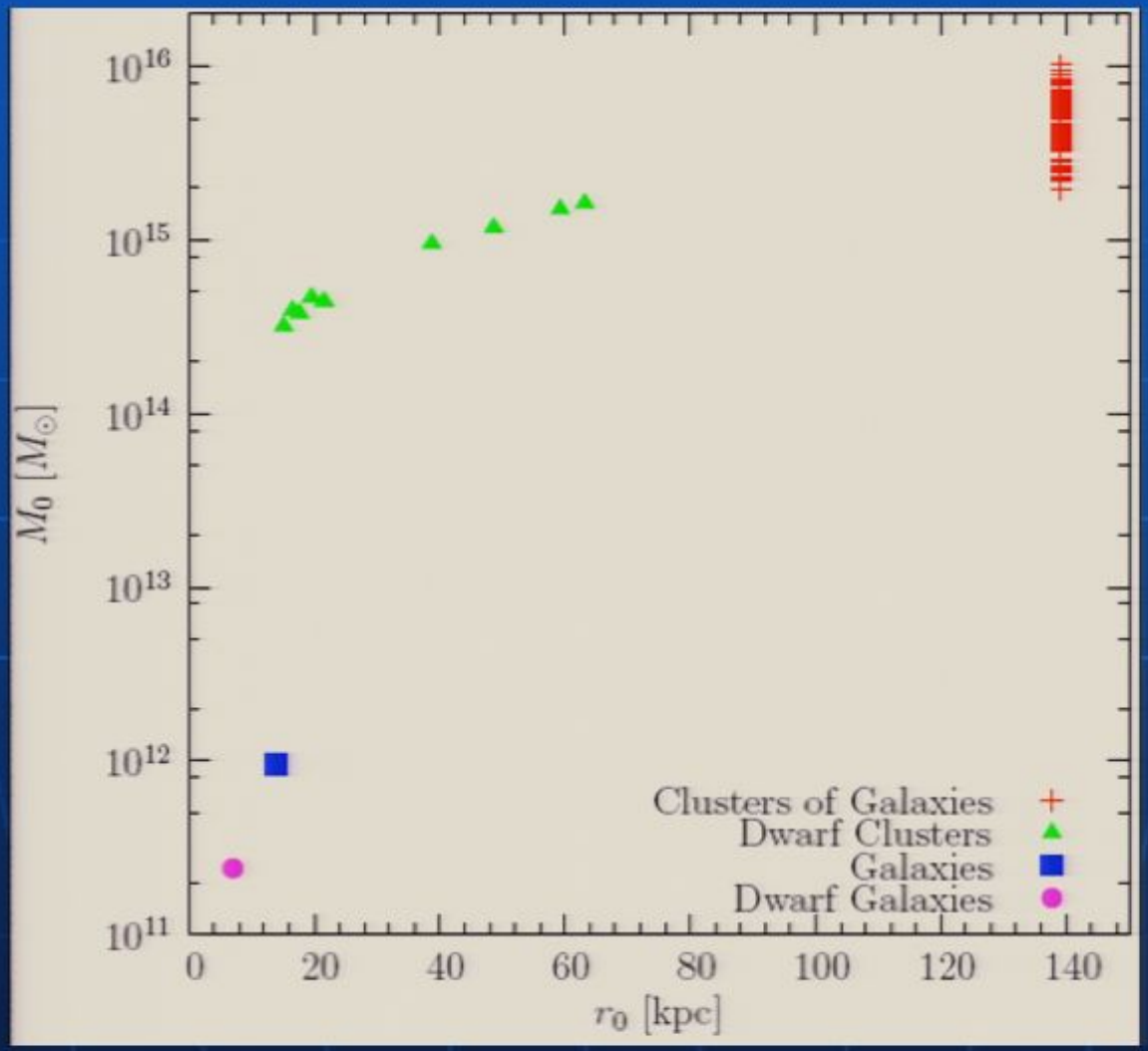

2. Modified Gravity (MOG)

Our STVG action takes the form $S = S_{\rm Grav} + S_\phi + S_S + S_M$

$$S_{\rm Grav} = \frac{1}{16\pi}\int d^4x\sqrt{-g}\left[\frac{1}{G}(R+2\Lambda)\right],$$

$$S_\phi = -\int d^4x\sqrt{-g}\left[\omega\left(\frac{1}{4}B^{\mu\nu}B_{\mu\nu}+V(\phi)\right)\right],$$

$$S_S = \int d^4x\sqrt{-g}\left[\frac{1}{G^3}\left(\frac{1}{2}g^{\mu\nu}\nabla_\mu G\nabla_\nu G - V(G)\right)\right.$$

$$\left.+\frac{1}{G}\left(\frac{1}{2}g^{\mu\nu}\nabla_\mu\omega\nabla_\nu\omega - V(\omega)\right)+\frac{1}{\mu^2 G}\left(\frac{1}{2}g^{\mu\nu}\nabla_\mu\mu\nabla_\nu\mu - V(\mu)\right)\right]$$

- Metric $g_{\mu\nu}(x)$, massive vector field $\phi_\mu(x)$, 3 scalar fields $G(x)$, $\omega(x)$ and $\mu(x)$.

The modified weak field acceleration law is given by

$$a(r) = -\frac{G(r)M}{r^2}$$

$$G(r) = G_0\left[1+\alpha(r)\left(1-\exp(-r/\lambda(r))\left(1+\frac{r}{\lambda(r)}\right)\right)\right]$$

Renormalization group (RG) flow "running" of $\alpha(r) = (M_0(r)/M)^{1/2} = f(\delta(r)/\mu_\alpha)$ and $\lambda(r) = 1/r_0(r) = h(\zeta(r)/\mu_\lambda)$.

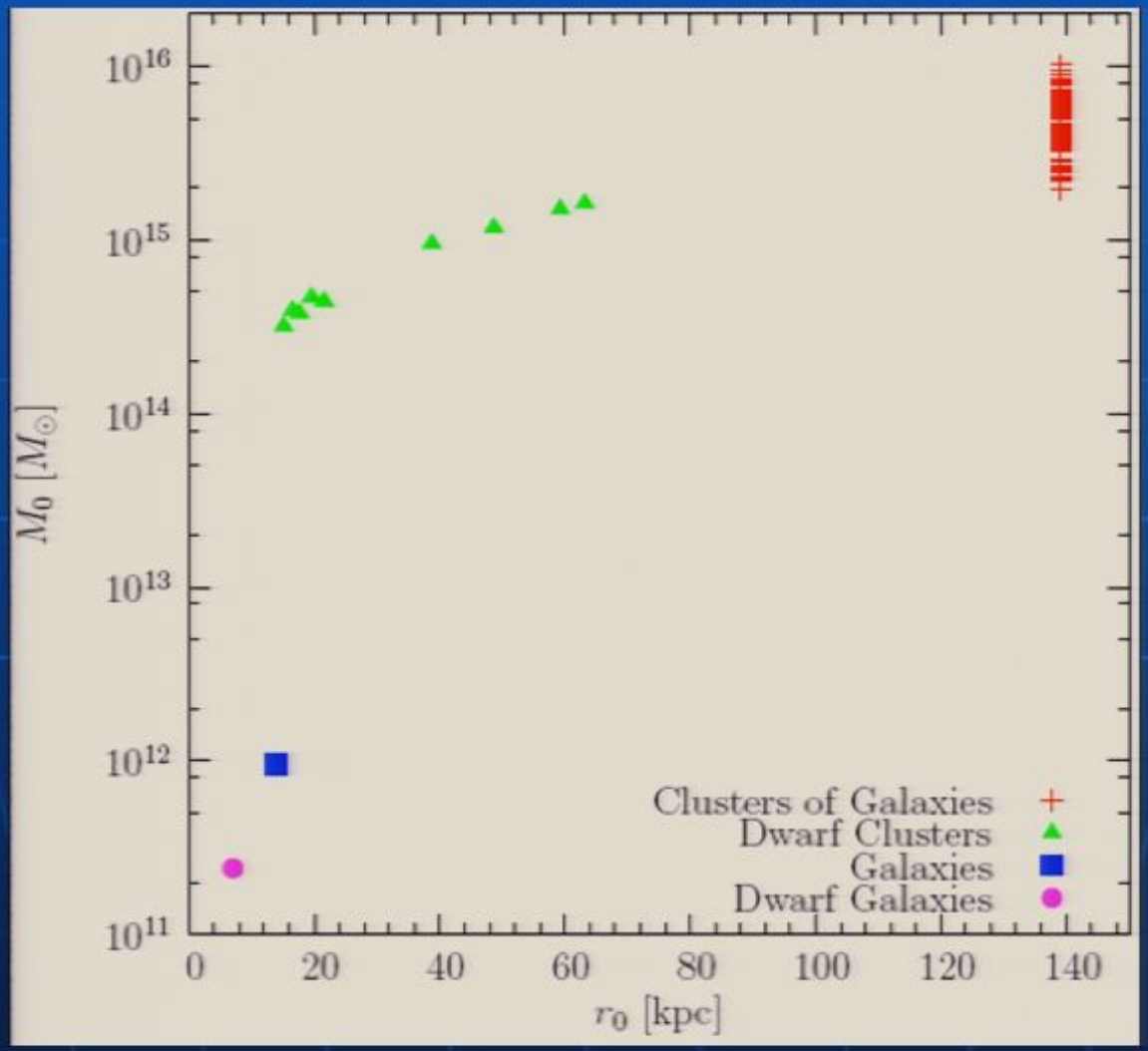

4. Fitting Galaxy Rotation Curves and Clusters

• A fitting routine has been applied to fit a large number of galaxy rotation curves (101 galaxies), using photometric data (58 galaxies) and a core model (43 galaxies) (Brownstein and JWM, 2005). The fits to the data are remarkably good and for the photometric data only one parameter, the mass-to-light ratio M/L, is used for the fitting once two parameters α and λ are universally fixed for galaxies and dwarf galaxies.

• The fits are close to those obtained from Milgrom's MOND acceleration law (Milgrom 1983) in all cases considered. A large sample of X-ray mass profile cluster data (106 clusters) has also been well fitted (Brownstein and JWM, 2005). The fitting of the radial dependence of the dynamical cluster mass is effectively a zero-parameter fit, for the two parameters α and λ are fitted to the determined bulk mass.

4. Fitting Galaxy Rotation Curves and Clusters

• A fitting routine has been applied to fit a large number of galaxy rotation curves (101 galaxies), using photometric data (58 galaxies) and a core model (43 galaxies) (Brownstein and JWM, 2005). The fits to the data are remarkably good and for the photometric data only one parameter, the mass-to-light ratio M/L, is used for the fitting once two parameters α and λ are universally fixed for galaxies and dwarf galaxies.

• The fits are close to those obtained from Milgrom's MOND acceleration law (Milgrom 1983) in all cases considered. A large sample of X-ray mass profile cluster data (106 clusters) has also been well fitted (Brownstein and JWM, 2005). The fitting of the radial dependence of the dynamical cluster mass is effectively a zero-parameter fit, for the two parameters α and λ are fitted to the determined bulk mass.

• The rotational velocity curves become the Kepler-Newtonian curves at large distances from the galaxies (satellites).

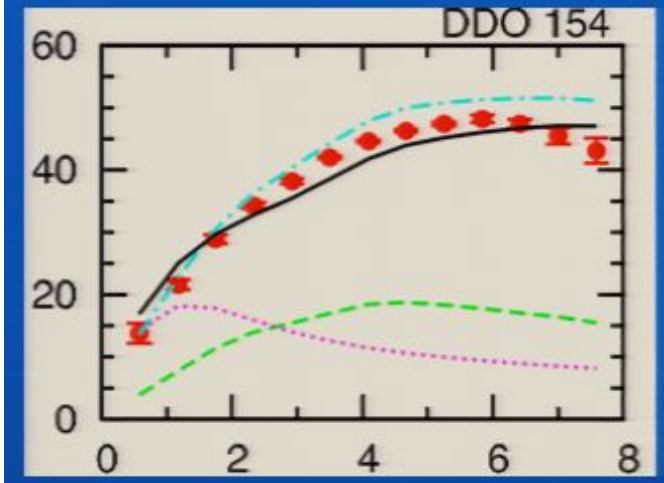

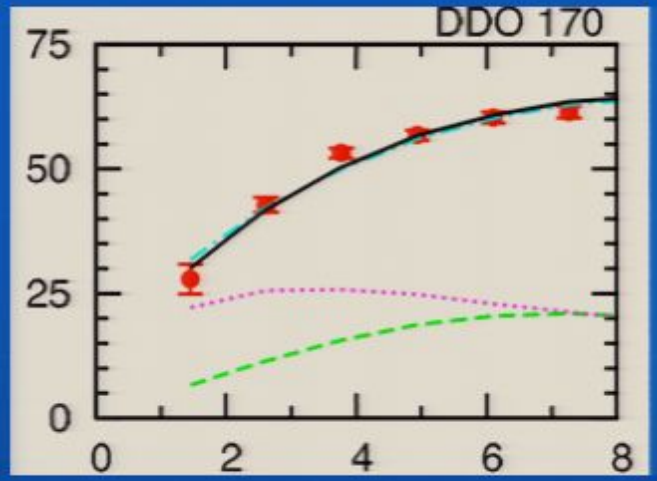

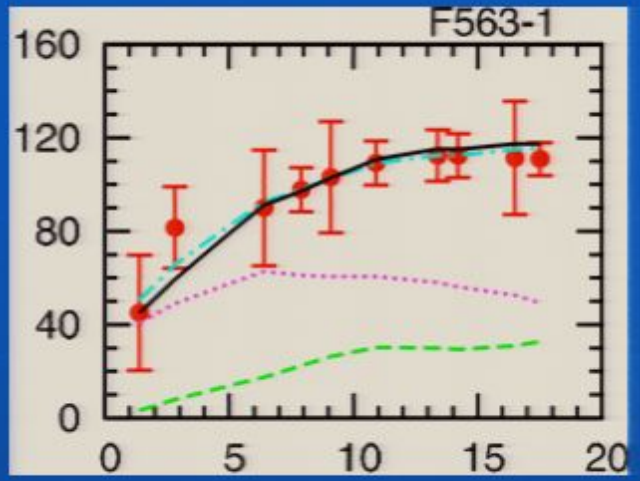

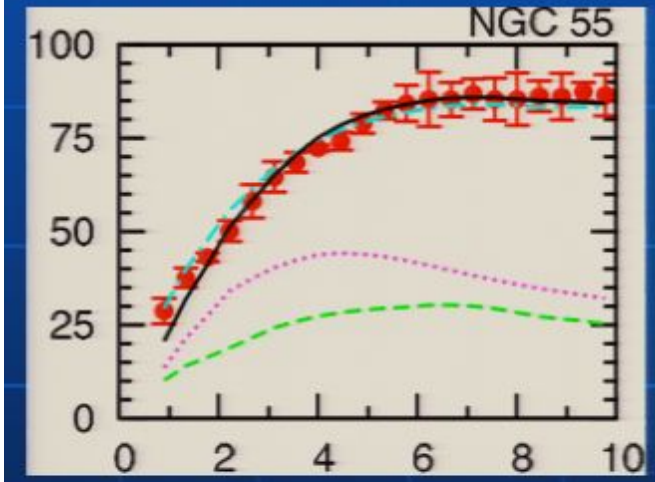

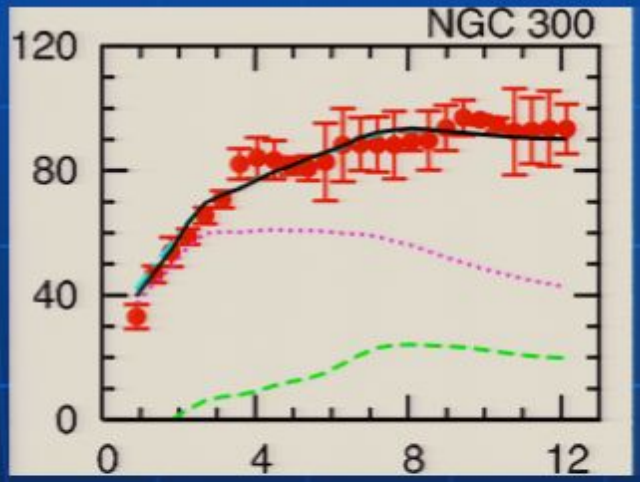

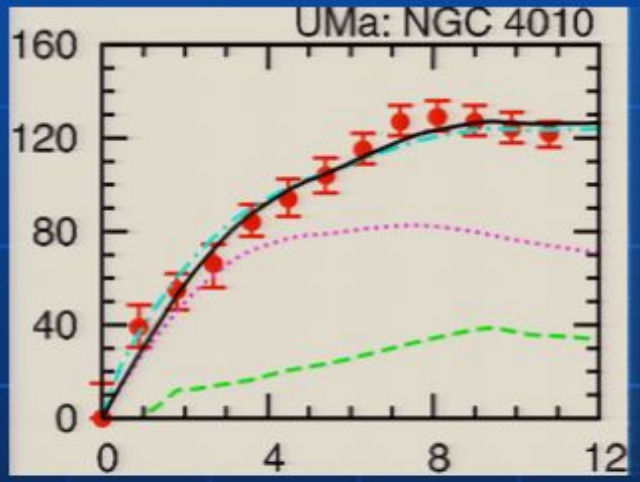

astro-ph/0506370 From 58 Photometric Fits: In all cases, the radial coordinate (horizontal axis) is given in kpc and the rotation velocity (vertical axis) in km/s. The red points with error bars are the observations, the solid black line is the rotation curve determined from MSTG, the dash-dot cyan line is the rotation curve determined from MOND. The other curves are the Newtonian rotation curves of the various separate components: the long dashed green line is the rotation curve of the gaseous disk (HI plus He); the dotted magenta curve is that of the luminous stellar disk.

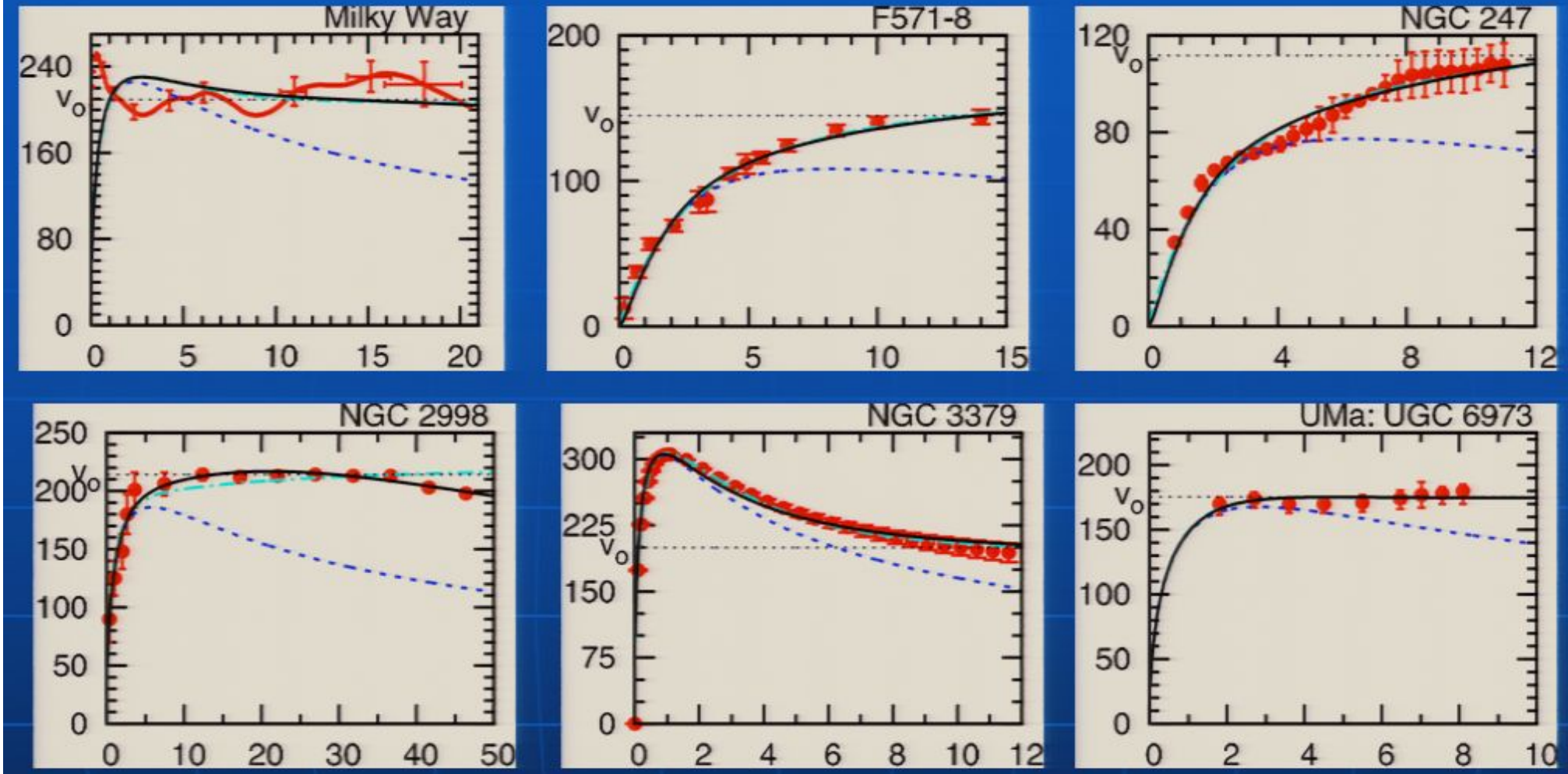

astro-ph/0506370 From 101 Parametric Fits: In all cases, the red points (with error bars) are the observations. The solid black line is the rotation curve determined from MSTG, the dash-dot cyan line is the rotation curve determined from MOND. The horizontal dotted black line is the MSTG predicted value of the measured "flat rotation velocity", v_0. The remaining curve – the short dashed blue line is the Newtonian galaxy rotation curve.

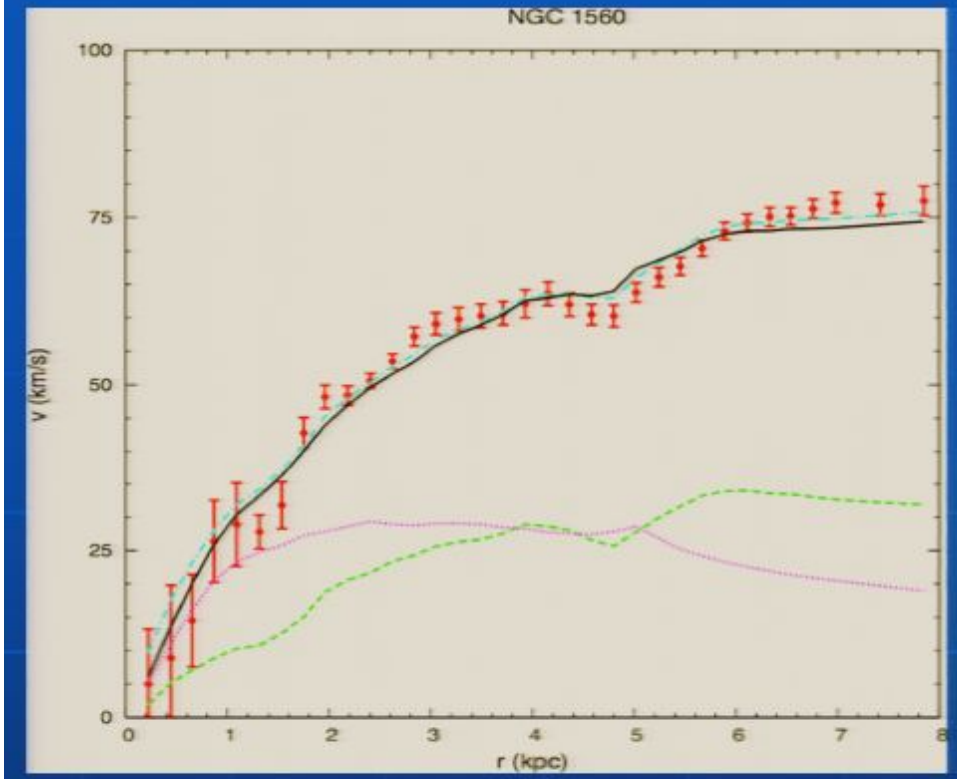

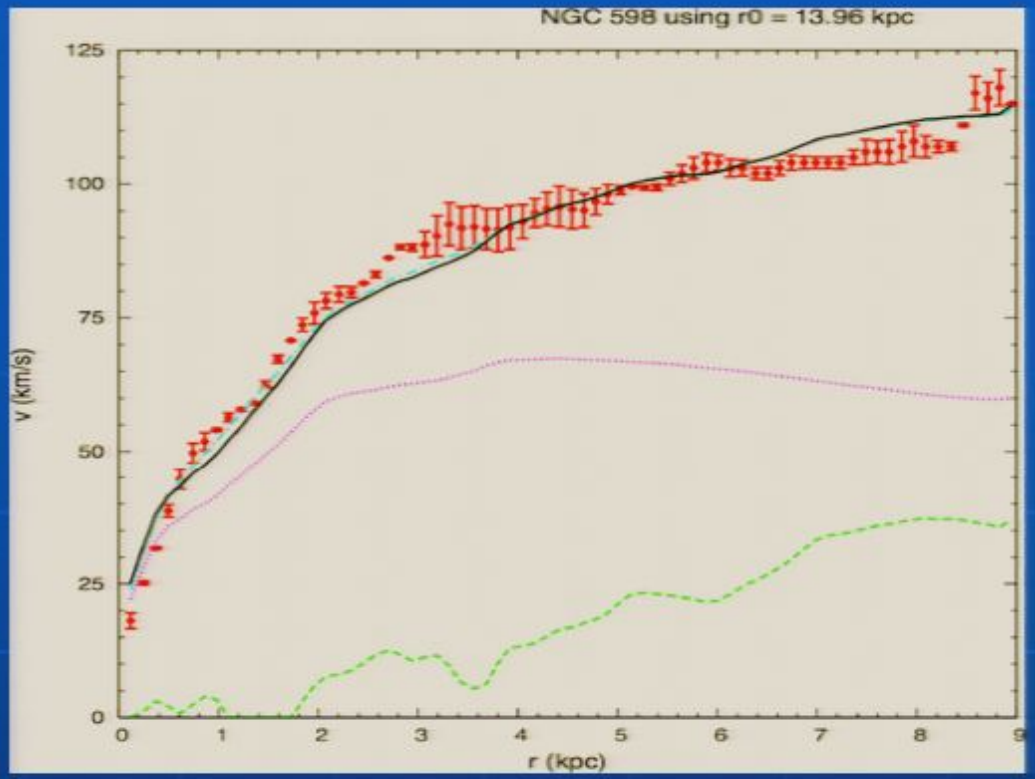

Photometric fits to galaxy rotation curves. There are 4 benchmark galaxies presented here; each is a best fit via the single parameter $(M/L)_{stars}$ based on the photometric data of the gaseous (HI plus He) and luminous stellar disks. The radial coordinate (**horizontal axis**) is given in kpc and the rotational velocity (**vertical axis**) in km/s. The red points with error bars are the observations, the solid black line is the rotation curve determined from MOG, and the dash-dotted cyan line is the rotation curve determined from MOND. The other curves are the Newtonian rotation curves of the various separate components: the long-dashed green line is the rotation curve of the gaseous disk (HI plus He), and the dotted magenta curve is that of the luminous stellar disk.

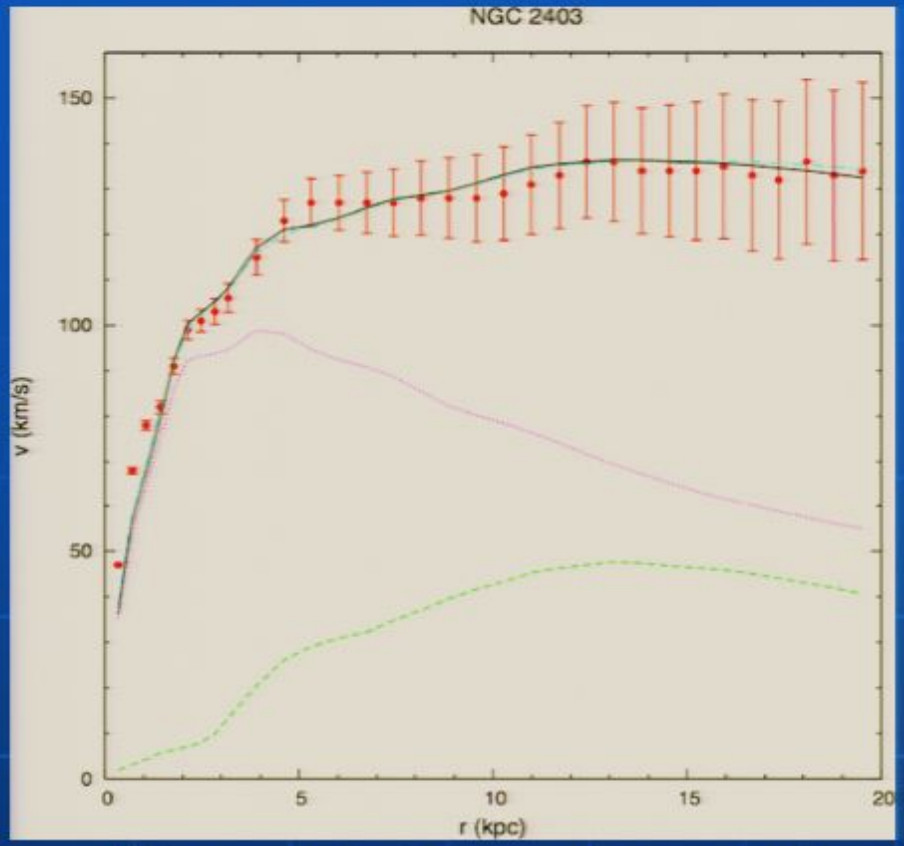

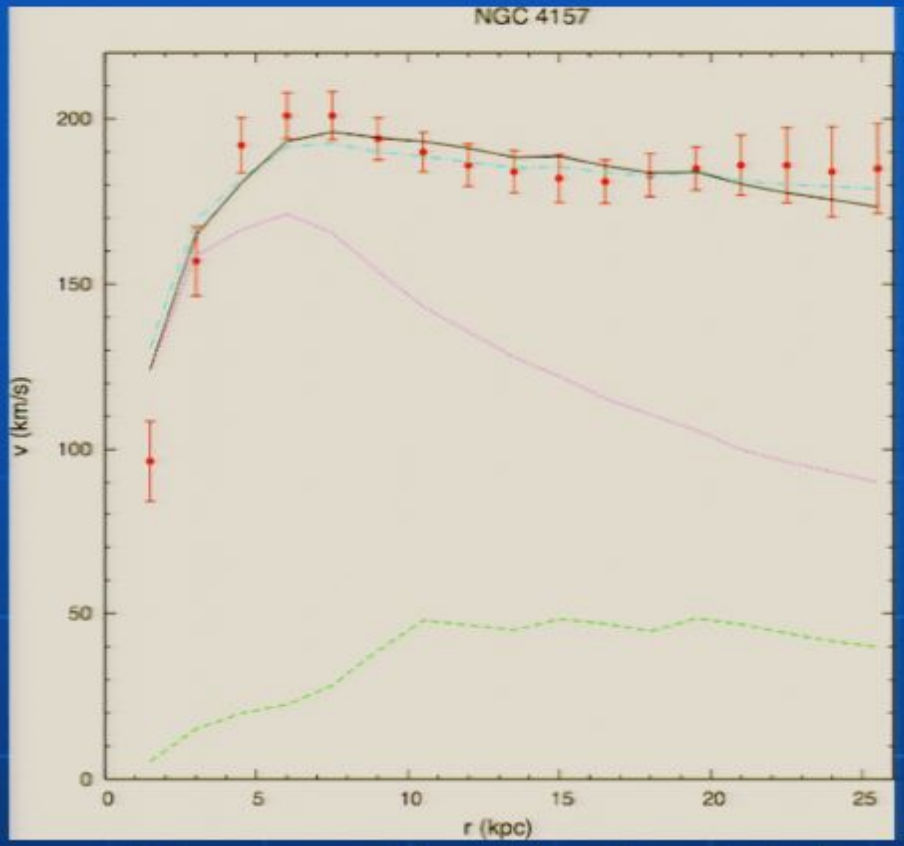

Photometric fits to galaxy rotation curves. There are 4 benchmark galaxies presented here; each is a best fit via the single parameter $(M/L)_{stars}$ based on the photometric data of the gaseous (HI plus He) and luminous stellar disks. The radial coordinate (**horizontal axis**) is given in kpc and the rotational velocity (**vertical axis**) in km/s. The red points with error bars are the observations, the solid black line is the rotation curve determined from MOG, and the dash-dotted cyan line is the rotation curve determined from MOND. The other curves are the Newtonian rotation curves of the various separate components: the long-dashed green line is the rotation curve of the gaseous disk (HI plus He), and the dotted magenta curve is that of the luminous stellar disk.

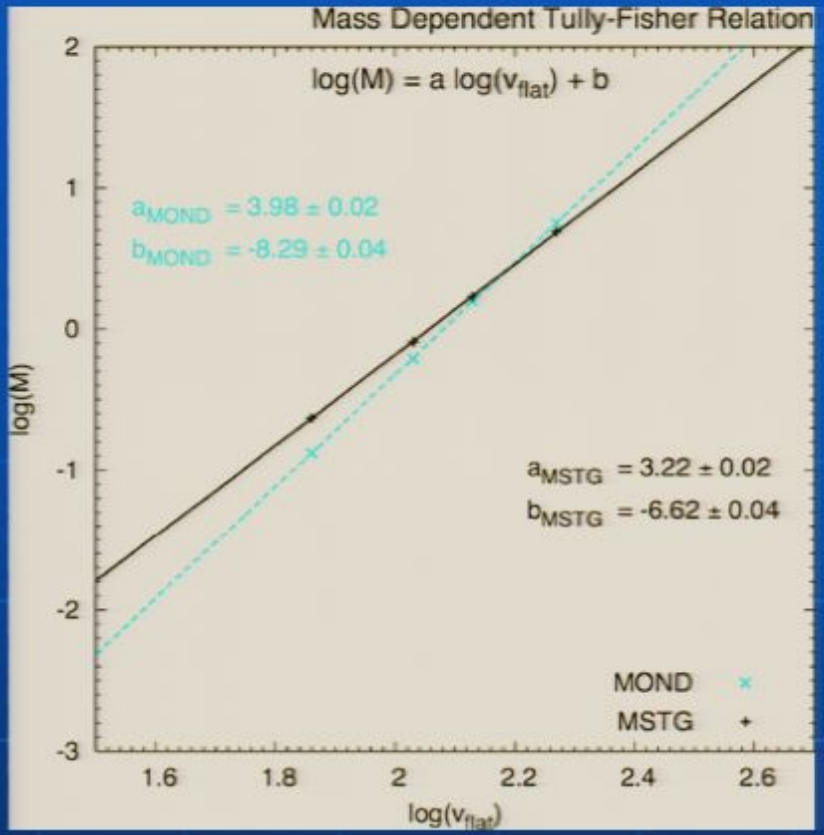

Mass dependent Tully-Fisher relation for the photometry of the 4 benchmark of galaxies. The **vertical axis** is the (base 10) logarithm of the total mass of the galaxy (in $10^{10} M_{\odot}$) resulting from the respective fits. The **horizontal axis** is the (base 10) logarithm of the flat rotational velocity (in km/s) as determined from the fits. The cyan crosses are the MOND results, and the black plus signs are the MSTG results. The Tully-Fisher relation is parametrized by $\log(M) = a\log(v)+b$, and the best-fit results using a nonlinear least-squares fitting routine including estimated errors are shown for MSTG and MOND. The dashed cyan line is the best-fit solution for the MOND results, and the solid black line is the best-fit solution for MSTG results.

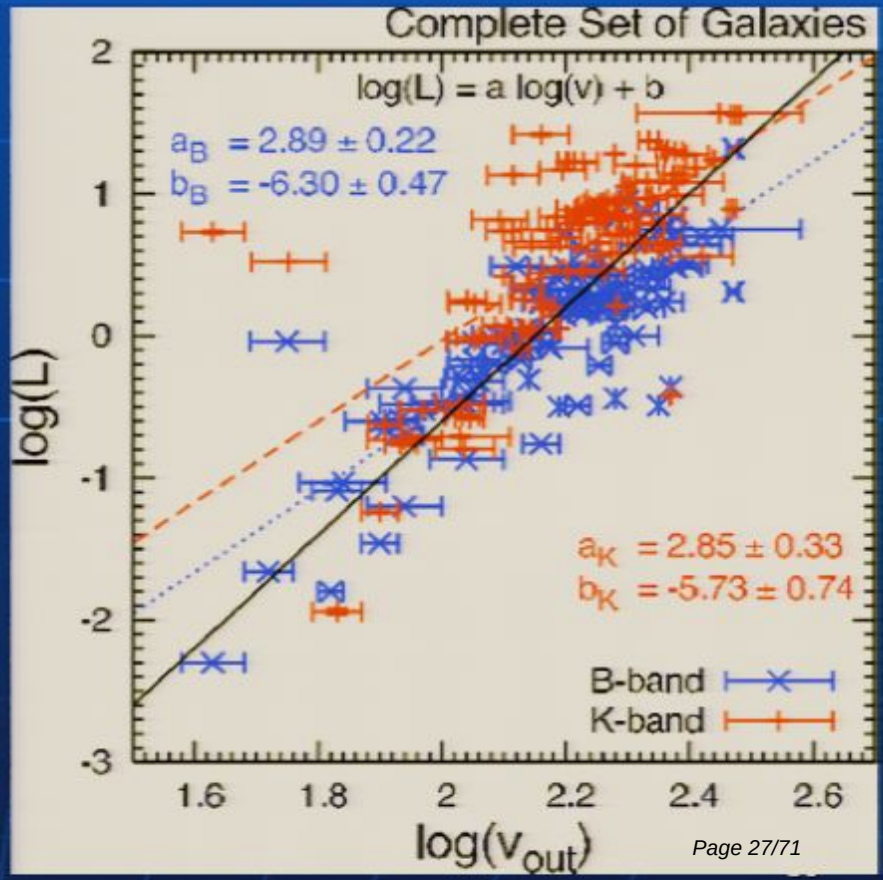

Observed B-band K-band Tully-Fisher relation for the Complete Set of galaxies of J. R. Brownstein & J. W. Moffat (2006) Astrophys. J. **636** 721. The **vertical axis** is the (base 10) logarithm of the observed galaxy luminosity (in $10^{10} L_{\odot}$), and the **horizontal axis** is the (base 10) logarithm of the observed rotational velocity (in km/s) at the maximum observed radius. The blue crosses are the observed B-band luminosity data and the red plus signs are the observed K-band luminosity data. The Tully-Fisher relation is parametrized by $\log(L) = a\log(v) + b$. The blue dotted line is the best-fit B-band Tully-Fisher relation and the red dashed line is the best-fit K-band Tully-Fisher relation. The solid black line is the MOND prediction with $\langle M/L \rangle \equiv 1$.

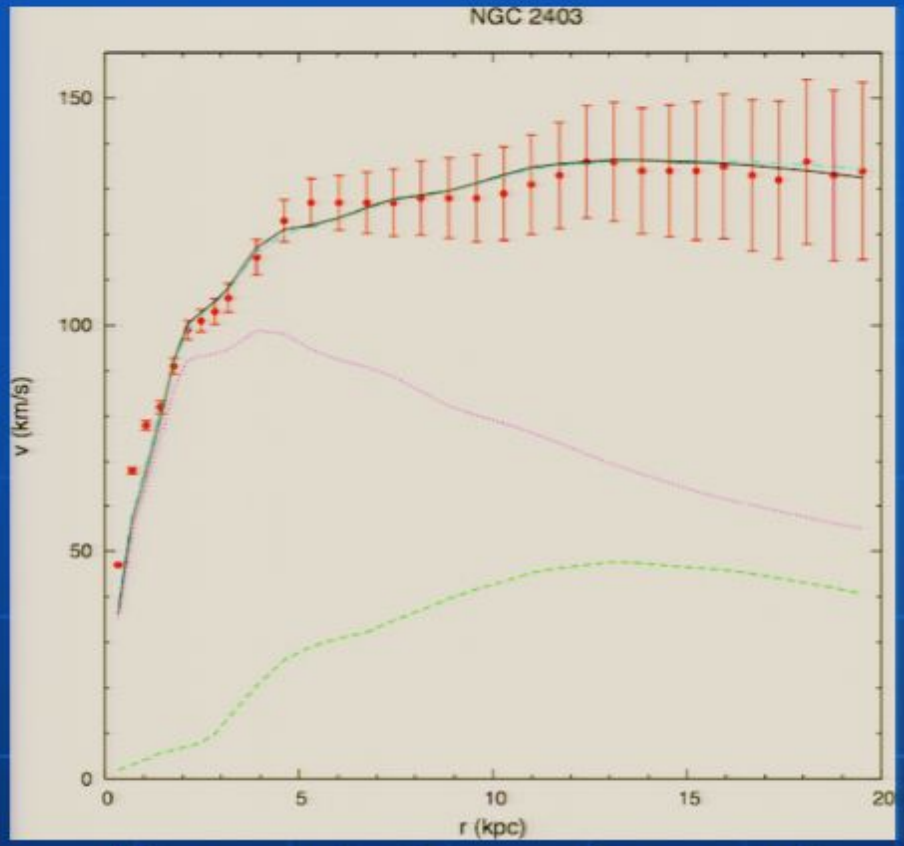

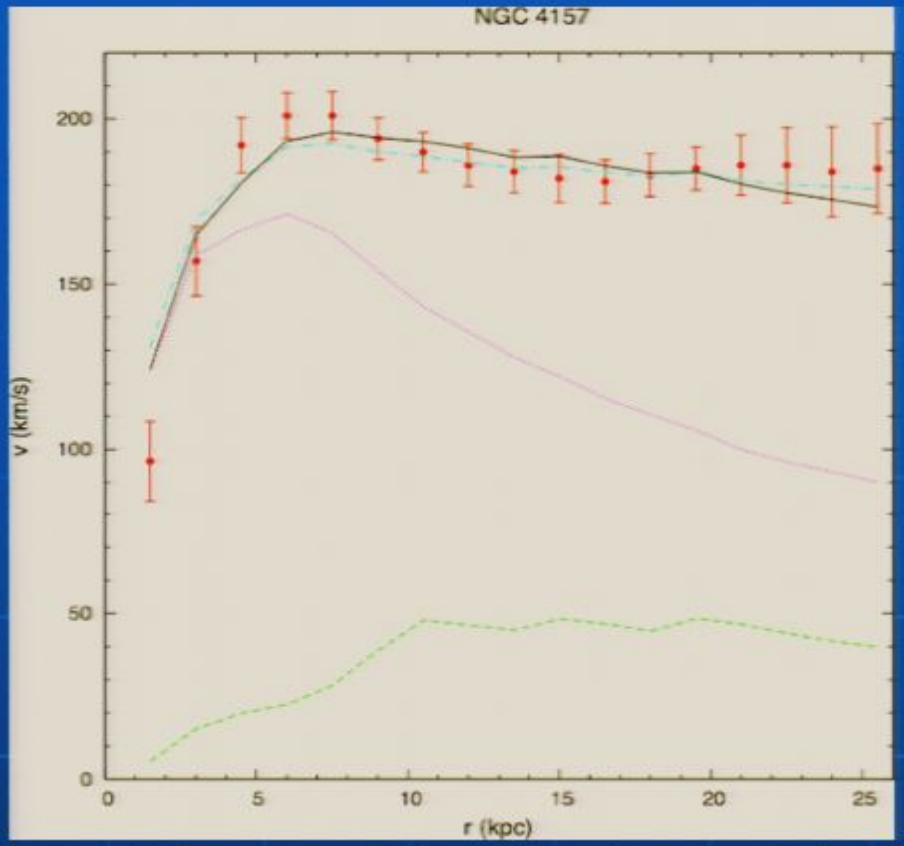

Photometric fits to galaxy rotation curves. There are 4 benchmark galaxies presented here; each is a best fit via the single parameter $(M/L)_{stars}$ based on the photometric data of the gaseous (HI plus He) and luminous stellar disks. The radial coordinate (**horizontal axis**) is given in kpc and the rotational velocity (**vertical axis**) in km/s. The red points with error bars are the observations, the solid black line is the rotation curve determined from MOG, and the dash-dotted cyan line is the rotation curve determined from MOND. The other curves are the Newtonian rotation curves of the various separate components: the long-dashed green line is the rotation curve of the gaseous disk (HI plus He), and the dotted magenta curve is that of the luminous stellar disk.

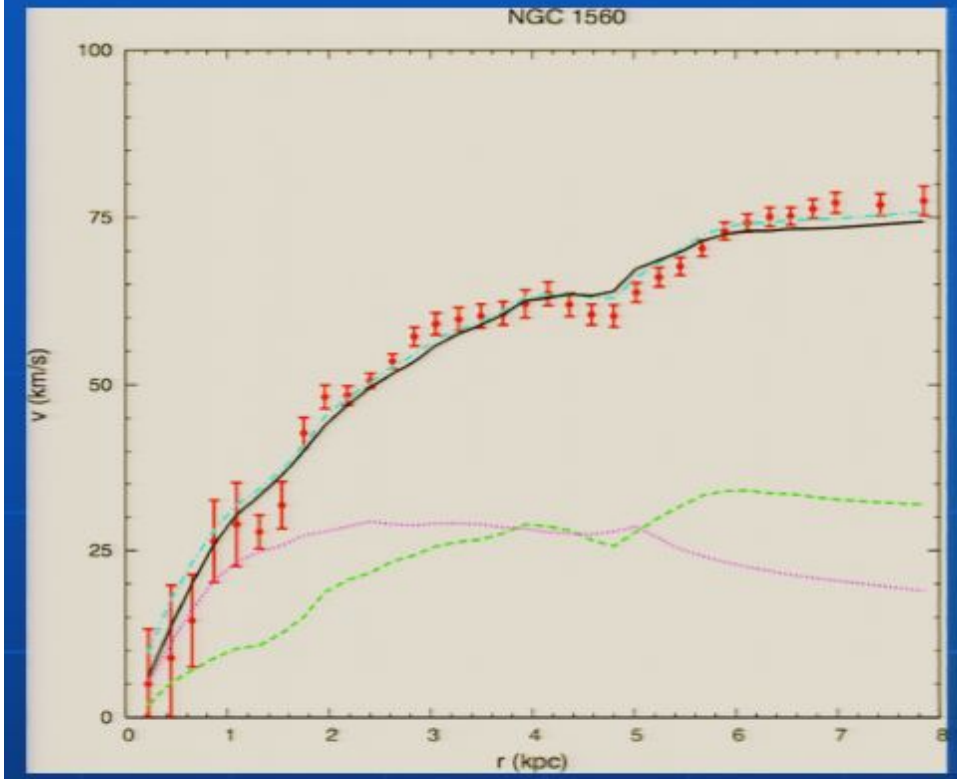

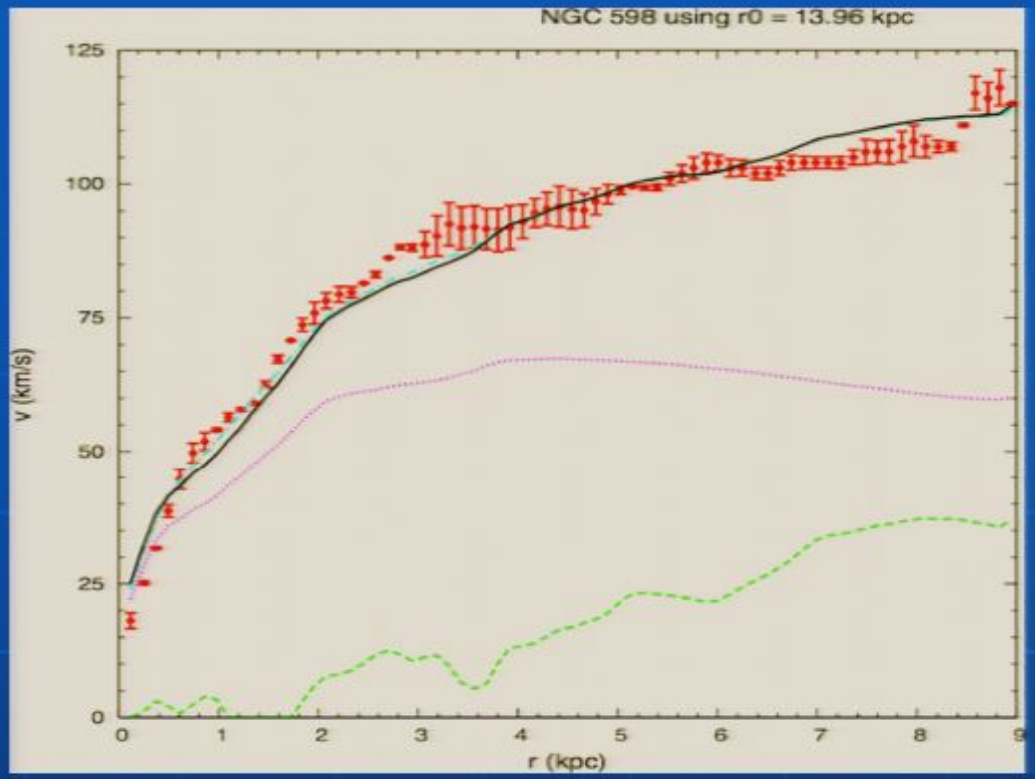

Photometric fits to galaxy rotation curves. There are 4 benchmark galaxies presented here; each is a best fit via the single parameter $(M/L)_{stars}$ based on the photometric data of the gaseous (HI plus He) and luminous stellar disks. The radial coordinate (**horizontal axis**) is given in kpc and the rotational velocity (**vertical axis**) in km/s. The red points with error bars are the observations, the solid black line is the rotation curve determined from MOG, and the dash-dotted cyan line is the rotation curve determined from MOND. The other curves are the Newtonian rotation curves of the various separate components: the long-dashed green line is the rotation curve of the gaseous disk (HI plus He), and the dotted magenta curve is that of the luminous stellar disk.

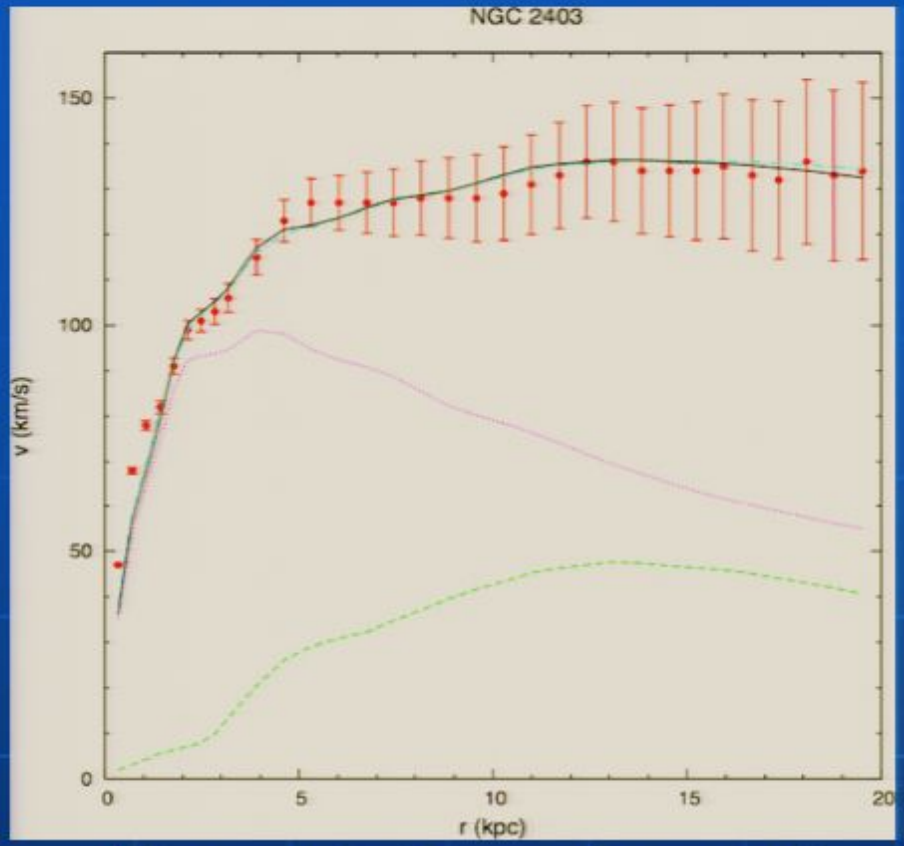

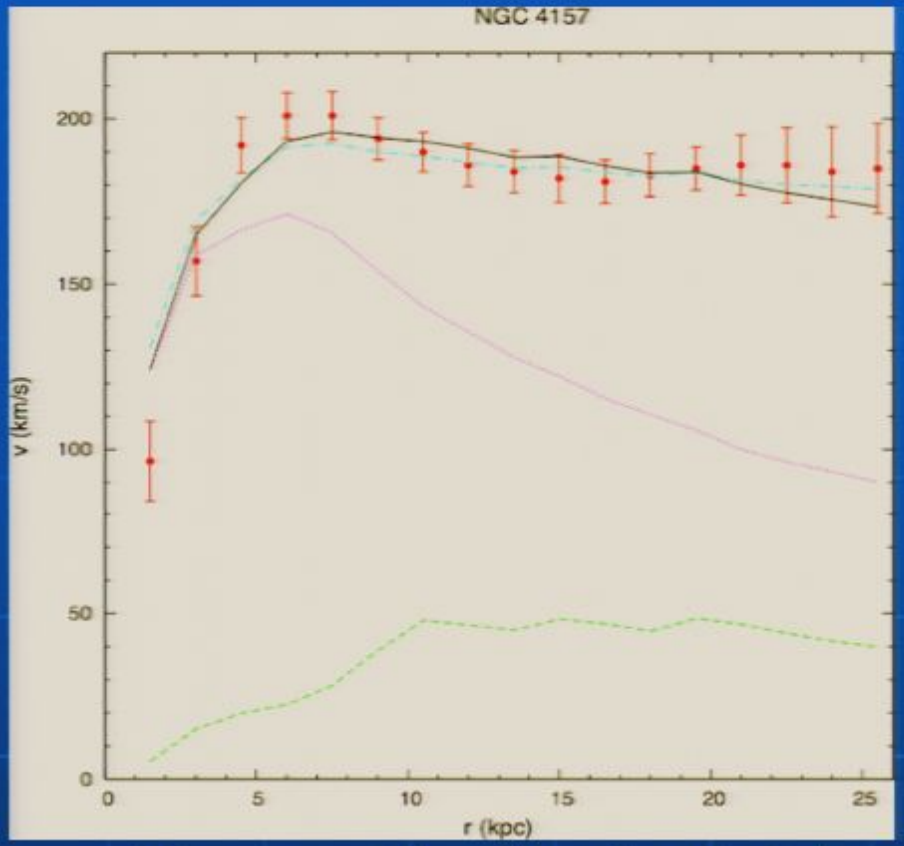

Photometric fits to galaxy rotation curves. There are 4 benchmark galaxies presented here; each is a best fit via the single parameter $(M/L)_{stars}$ based on the photometric data of the gaseous (HI plus He) and luminous stellar disks. The radial coordinate (**horizontal axis**) is given in kpc and the rotational velocity (**vertical axis**) in km/s. The red points with error bars are the observations, the solid black line is the rotation curve determined from MOG, and the dash-dotted cyan line is the rotation curve determined from MOND. The other curves are the Newtonian rotation curves of the various separate components: the long-dashed green line is the rotation curve of the gaseous disk (HI plus He), and the dotted magenta curve is that of the luminous stellar disk.

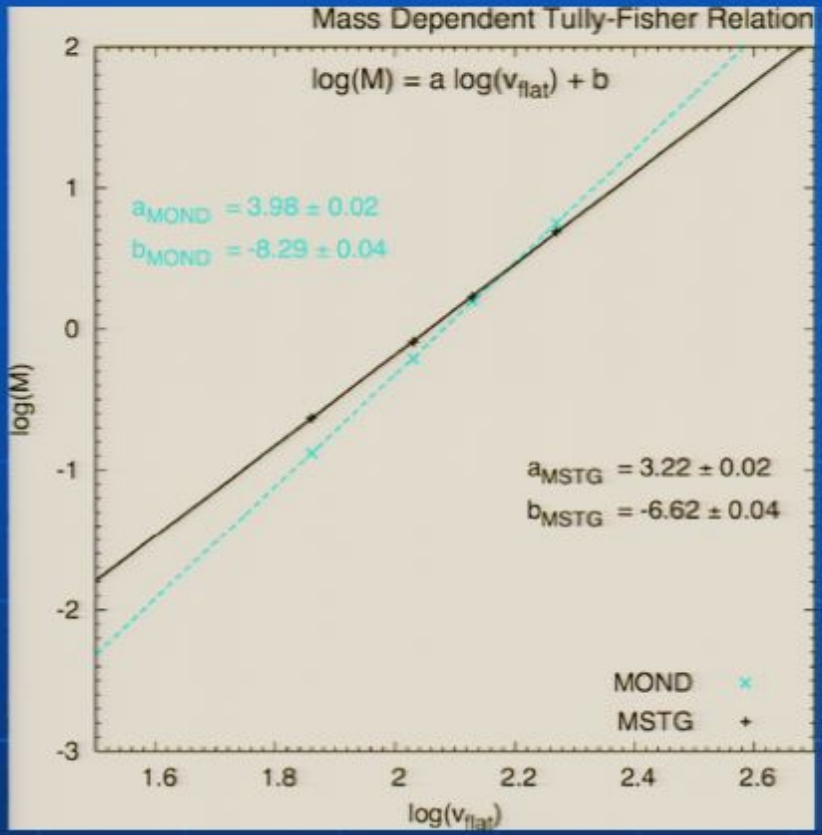

Mass dependent Tully-Fisher relation for the photometry of the 4 benchmark of galaxies. The **vertical axis** is the (base 10) logarithm of the total mass of the galaxy (in $10^{10} M_{\odot}$) resulting from the respective fits. The **horizontal axis** is the (base 10) logarithm of the flat rotational velocity (in km/s) as determined from the fits. The cyan crosses are the MOND results, and the black plus signs are the MSTG results. The Tully-Fisher relation is parametrized by $\log(M) = a \log(v) + b$, and the best-fit results using a nonlinear least-squares fitting routine including estimated errors are shown for MSTG and MOND. The dashed cyan line is the best-fit solution for the MOND results, and the solid black line is the best-fit solution for MSTG results.

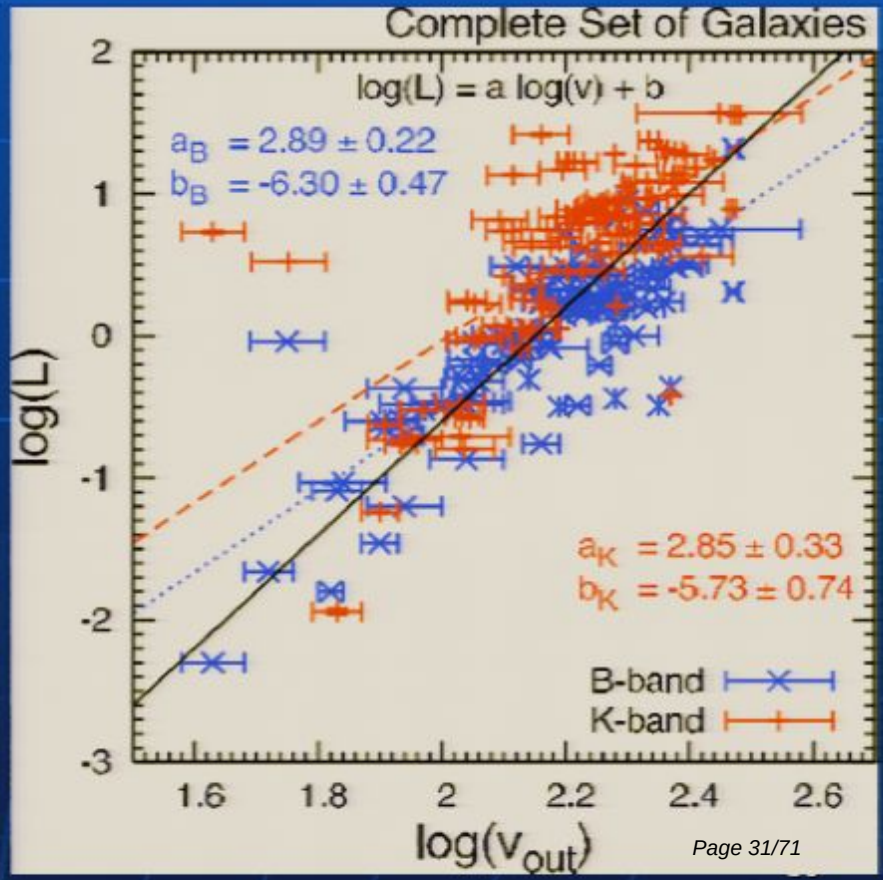

Observed B-band K-band Tully-Fisher relation for the Complete Set of galaxies of J. R. Brownstein & J. W. Moffat (2006) Astrophys. J. **636** 721. The **vertical axis** is the (base 10) logarithm of the observed galaxy luminosity (in $10^{10} L_{\odot}$), and the **horizontal axis** is the (base 10) logarithm of the observed rotational velocity (in km/s) at the maximum observed radius. The blue crosses are the observed B-band luminosity data and the red plus signs are the observed K-band luminosity data. The Tully-Fisher relation is parametrized by $\log(L) = a \log(v) + b$. The blue dotted line is the best-fit B-band Tully-Fisher relation and the red dashed line is the best-fit K-band Tully-Fisher relation. The solid black line is the MOND prediction with $\langle M/L \rangle \equiv 1$.

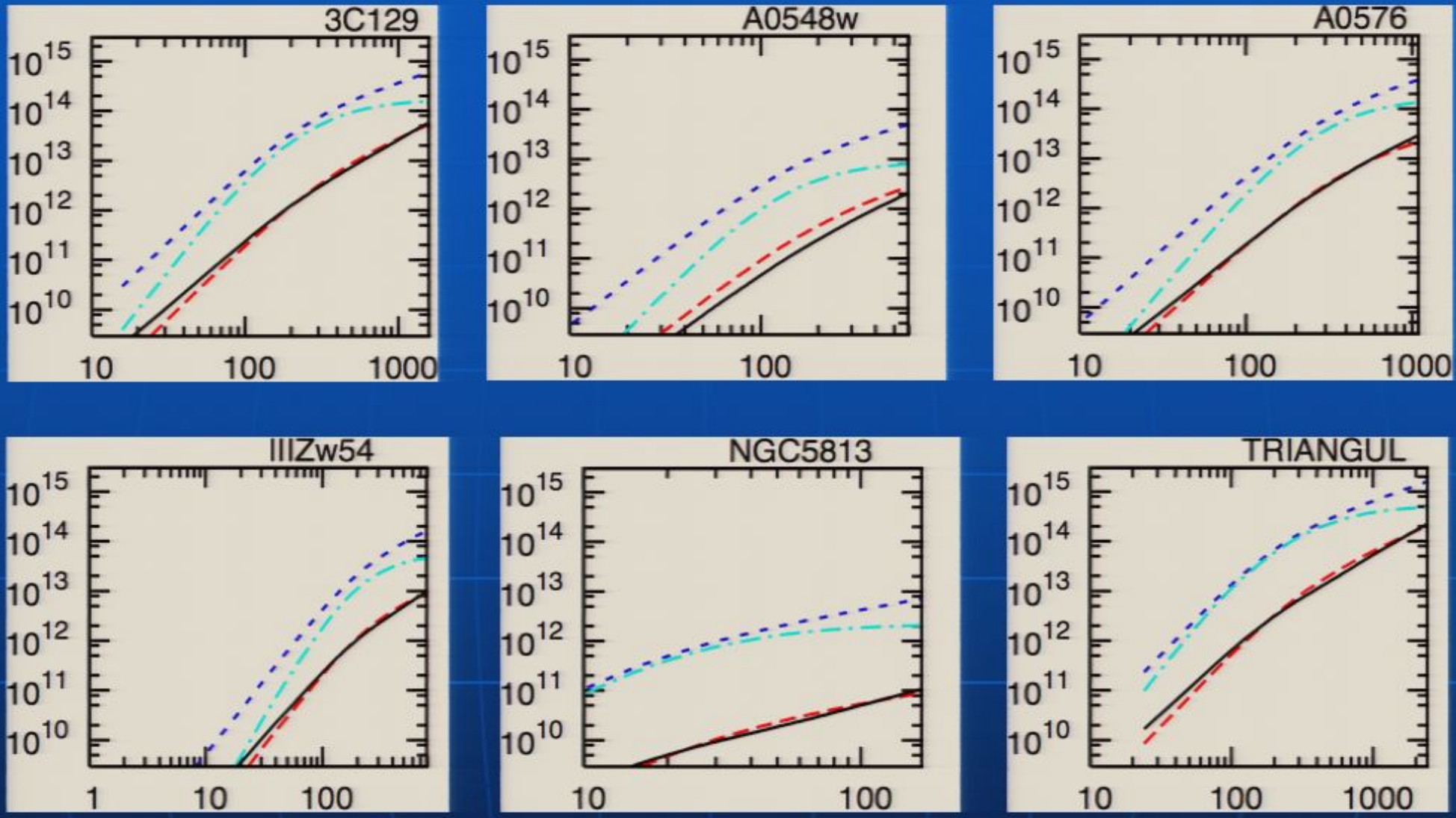

astro-ph/0507222 From 106 Cluster Fits: In all cases, the horizontal axis is the radius in kpc and the vertical axis is mass in units of $M_\odot$. The red long dashed curve is the ICM gas mass inferred from X-ray observations; the short dashed blue curve is the Newtonian dynamic mass; the dashed-dotted cyan curve is the MOND dynamic mass; and the solid black curve is the MSTG dynamic mass. The Newtonian, MOND and MSTG dynamic masses are calculated within the context of the $\beta-$model isothermal, isotropic sphere.

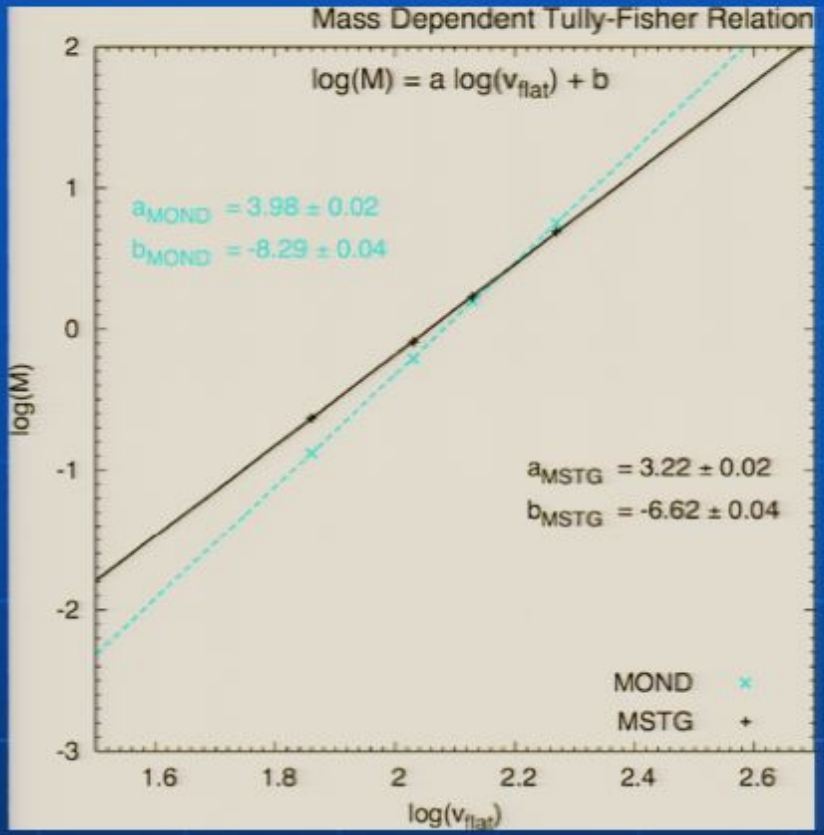

Mass dependent Tully-Fisher relation for the photometry of the 4 benchmark of galaxies. The **vertical axis** is the (base 10) logarithm of the total mass of the galaxy (in $10^{10} M_{\odot}$) resulting from the respective fits. The **horizontal axis** is the (base 10) logarithm of the flat rotational velocity (in km/s) as determined from the fits. The cyan crosses are the MOND results, and the black plus signs are the MSTG results. The Tully-Fisher relation is parametrized by $\log(M) = a \log(v) + b$, and the best-fit results using a nonlinear least-squares fitting routine including estimated errors are shown for MSTG and MOND. The dashed cyan line is the best-fit solution for the MOND results, and the solid black line is the best-fit solution for MSTG results.

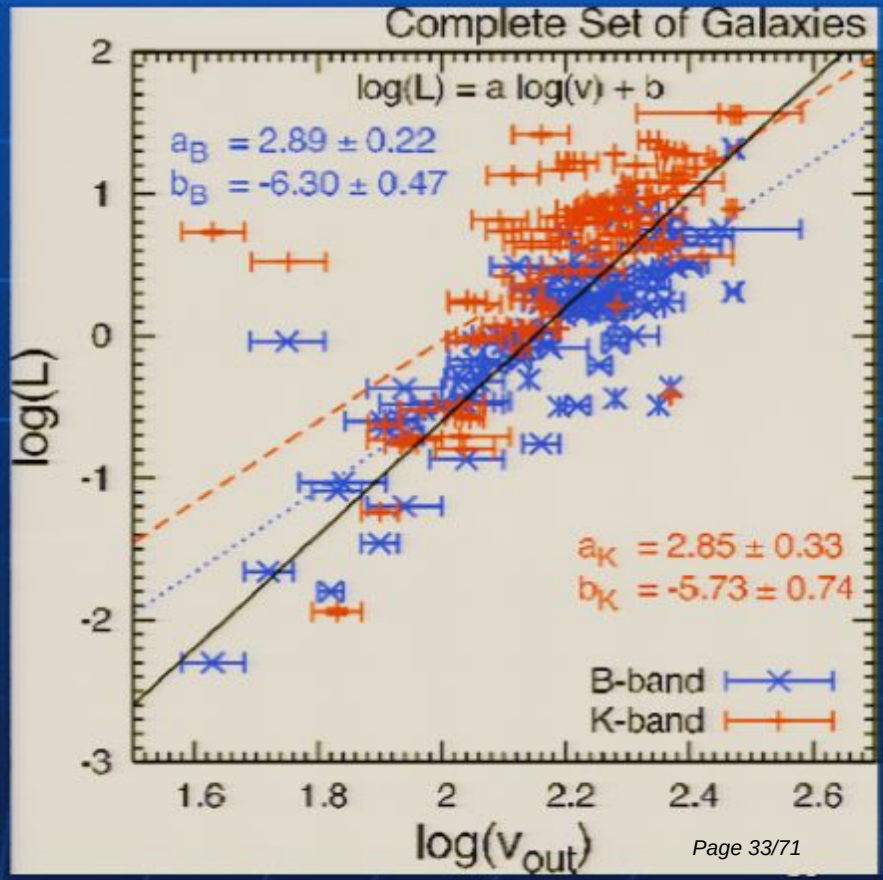

Observed B-band K-band Tully-Fisher relation for the Complete Set of galaxies of J. R. Brownstein & J. W. Moffat (2006) Astrophys. J. **636** 721. The **vertical axis** is the (base 10) logarithm of the observed galaxy luminosity (in $10^{10} L_{\odot}$), and the **horizontal axis** is the (base 10) logarithm of the observed rotational velocity (in km/s) at the maximum observed radius. The blue crosses are the observed B-band luminosity data and the red plus signs are the observed K-band luminosity data. The Tully-Fisher relation is parametrized by $\log(L) = a \log(v) + b$. The blue dotted line is the best-fit B-band Tully-Fisher relation and the red dashed line is the best-fit K-band Tully-Fisher relation. The solid black line is the MOND prediction with $\langle M/L \rangle \equiv 1$.

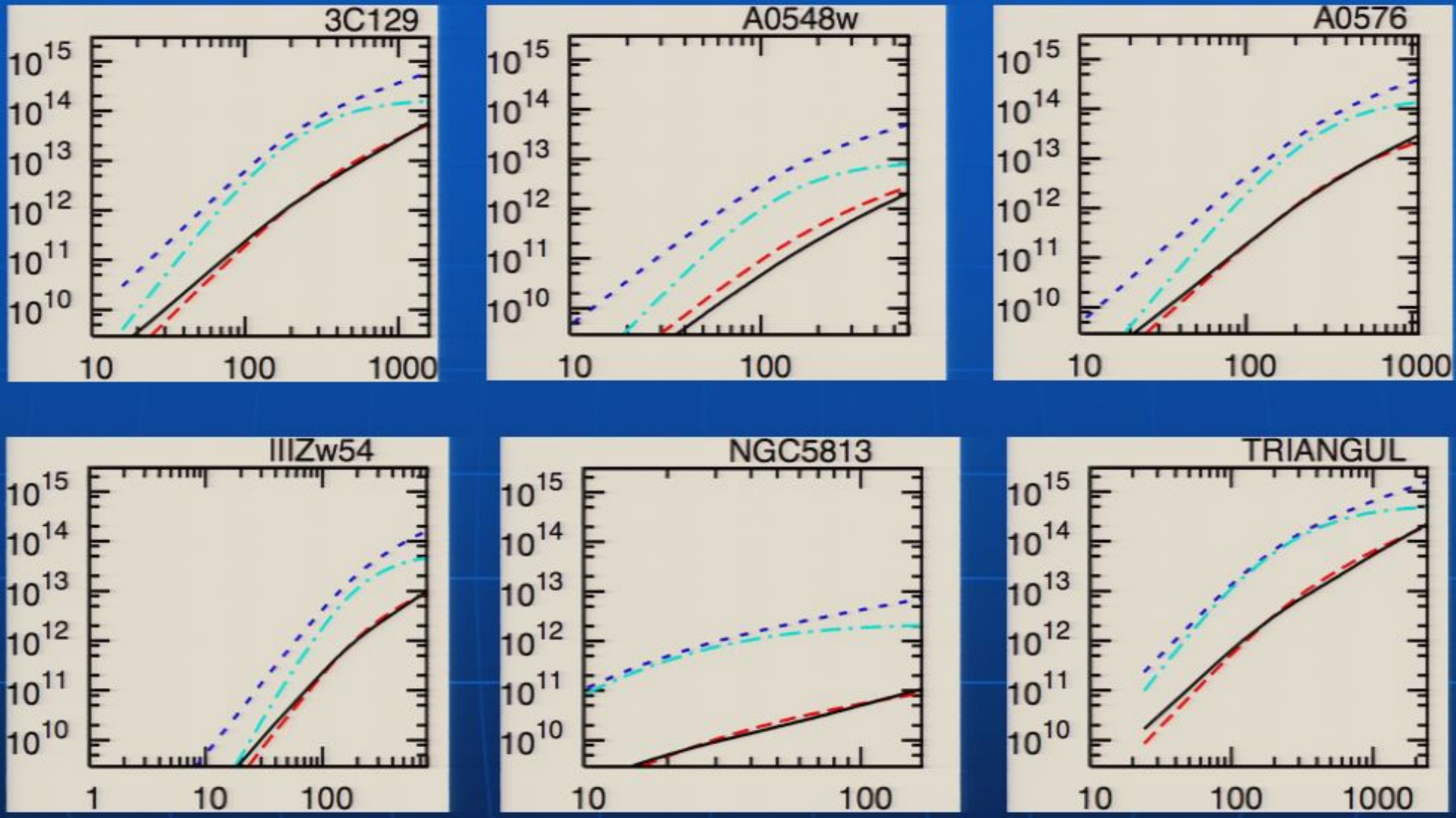

astro-ph/0507222 From 106 Cluster Fits: In all cases, the horizontal axis is the radius in kpc and the vertical axis is mass in units of $M_\odot$. The red long dashed curve is the ICM gas mass inferred from X-ray observations; the short dashed blue curve is the Newtonian dynamic mass; the dashed-dotted cyan curve is the MOND dynamic mass; and the solid black curve is the MSTG dynamic mass. The Newtonian, MOND and MSTG dynamic masses are calculated within the context of the $\beta-$model isothermal, isotropic sphere.

6. The Bullet Cluster

- The merging clusters 1E0657-56 (z= 0.296) (discovered by Tucker et al. 1995) is claimed to prove empirically the existence of dark matter (Clowe et al. 2003-2006, Bradac et al. 2006). Due to the collision of two clusters, the dissipationless stellar component and the X-ray emitting plasma are spatially segregated. The claim is that the gravitationally lensing maps show that that the gravitational potential does not trace the plasma distribution – the dominant baryonic mass component – but rather approximately traces the distribution of galaxies.

- *It is necessary in MOG to explain the 8σ significance spatial offset of the center of the total mass from the center of the baryonic mass peaks (JWM, 2006, J. R. Brownstein and JWM, 2006).*

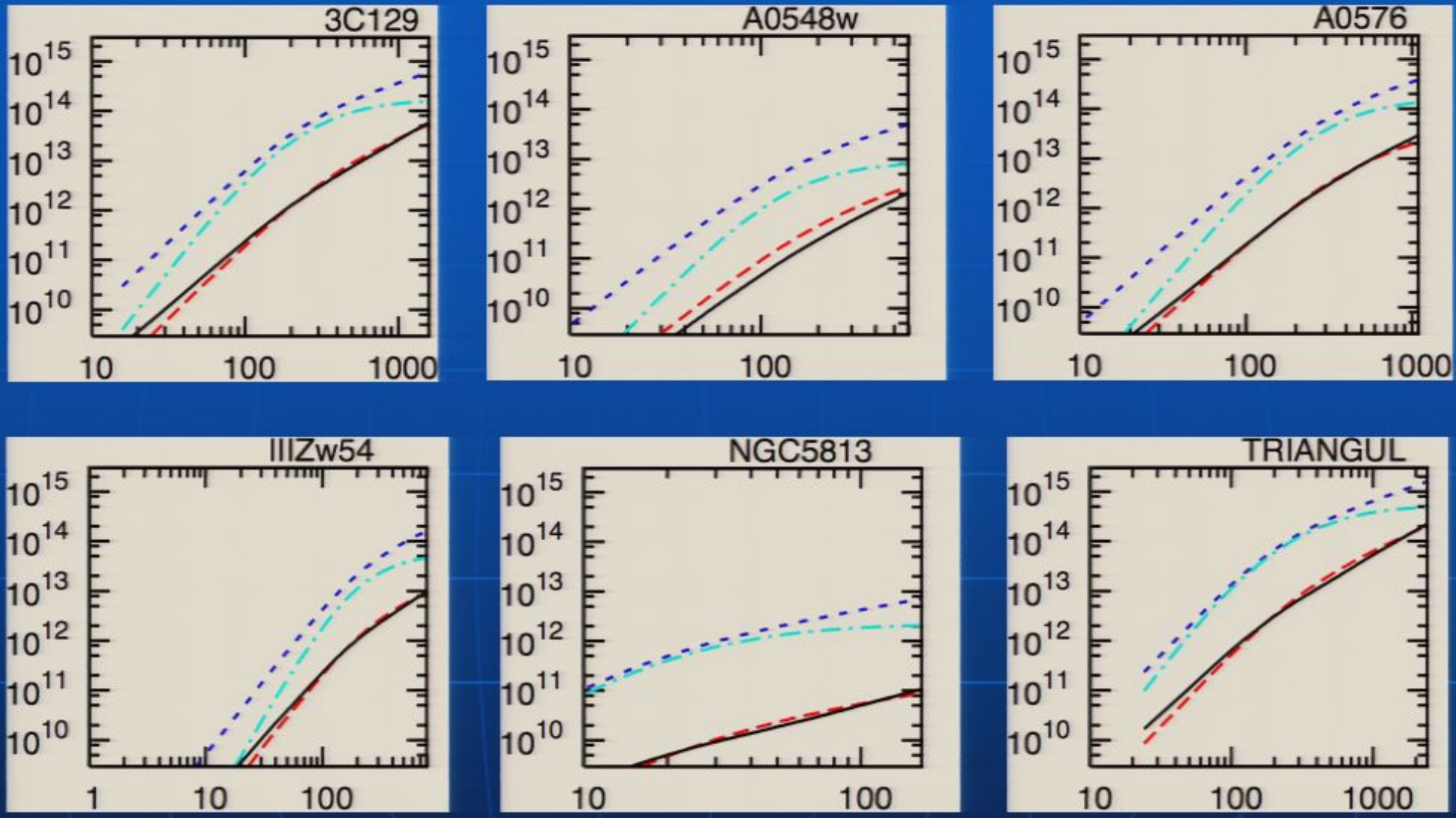

astro-ph/0507222 From 106 Cluster Fits: In all cases, the horizontal axis is the radius in kpc and the vertical axis is mass in units of $M_\odot$. The red long dashed curve is the ICM gas mass inferred from X-ray observations; the short dashed blue curve is the Newtonian dynamic mass; the dashed-dotted cyan curve is the MOND dynamic mass; and the solid black curve is the MSTG dynamic mass. The Newtonian, MOND and MSTG dynamic masses are calculated within the context of the $\beta-$model isothermal, isotropic sphere.

6. The Bullet Cluster

- The merging clusters 1E0657-56 (z= 0.296) (discovered by Tucker et al. 1995) is claimed to prove empirically the existence of dark matter (Clowe et al. 2003-2006, Bradac et al. 2006). Due to the collision of two clusters, the dissipationless stellar component and the X-ray emitting plasma are spatially segregated. The claim is that the gravitationally lensing maps show that that the gravitational potential does not trace the plasma distribution – the dominant baryonic mass component – but rather approximately traces the distribution of galaxies.

- *It is necessary in MOG to explain the 8σ significance spatial offset of the center of the total mass from the center of the baryonic mass peaks (JWM, 2006, J. R. Brownstein and JWM, 2006).*

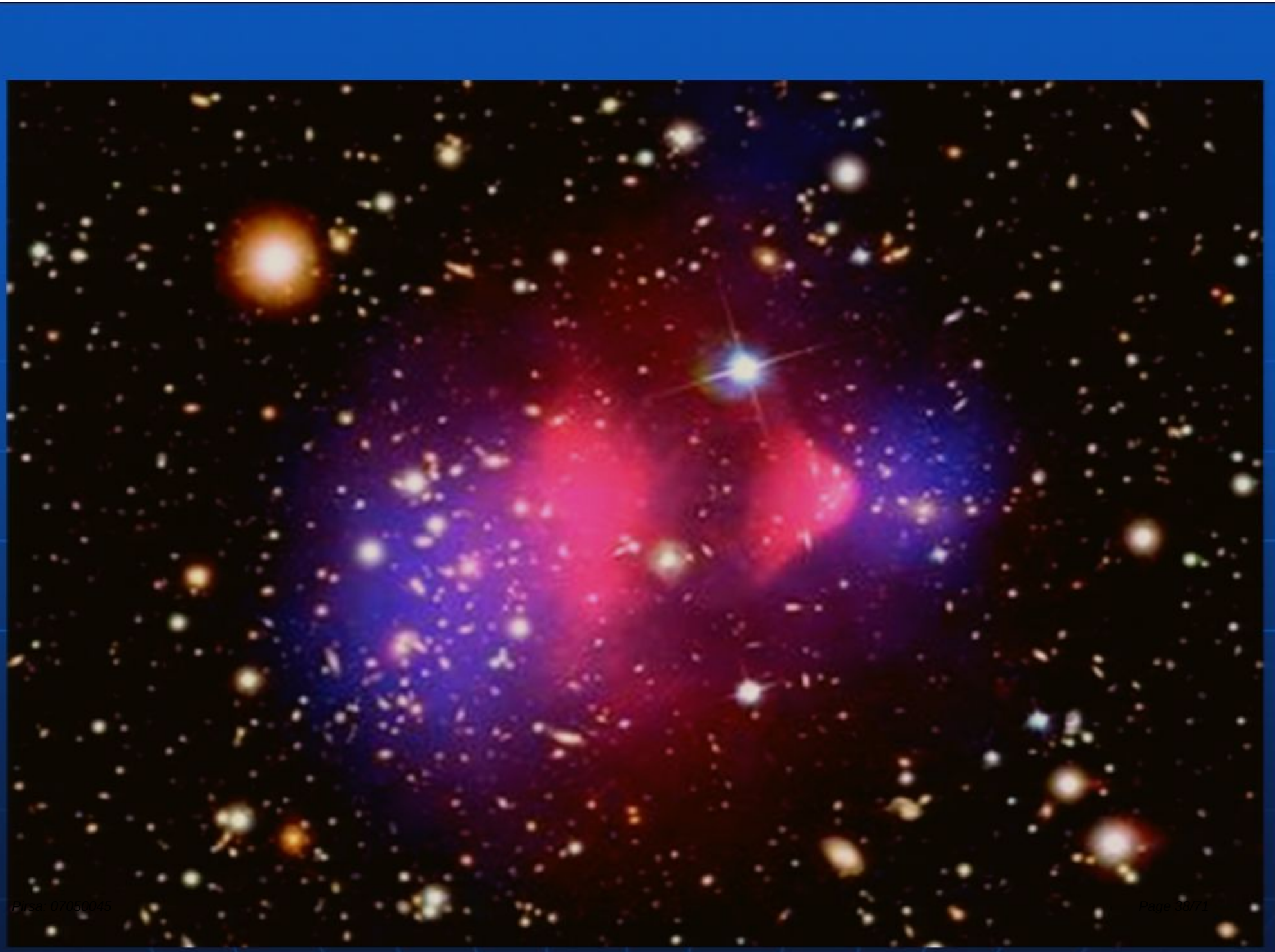

- The main cluster of E10657-56 is close to being isothermal, whereas the smaller bullet cluster is not isothermal and out of equilibrium (shock wave).

- Treat the subcluster as a perturbation, and neglect it at a zeroth order approximation.

- Include the subcluster as a perturbation, and shift the origin of the varying gravitational coupling G(r) toward the subcluster (toward the center-of-mass of the system).

- Use the concentric cylinder mass M(R) as an approximation for M(R), and shift that toward the subcluster (toward the MOG center).

- Treat the subcluster as a perturbation, and utilize the isothermal model to approximate M(R) and shift that towards the subcluster (towards the center-of-mass of the system – where the origin of G(r) is located).

• Starting with the zeroth order approximation, we neglect the subcluster, and perform a best-fit to determine a spherically symmetric King β model density of the main cluster. We assume that the main cluster gas is in nearly hydrostatic thermal equilibrium with the gravitational potential of the galaxy cluster.

$$\rho(r) = \rho_0 \left[1 + \left(\frac{r}{r_c}\right)^2\right]^{-3\beta/2}$$

$$M(r) = 4\pi \int_0^r \rho(r') r'^2 dr'$$

$$r_{\rm out} = r_c \left[\left(\frac{\rho_0}{10^{-28}\,{\rm g/cm^3}}\right)^{2/3\beta} - 1\right]^{1/2}$$

$$M_{\rm gas} = 4\pi \int_0^{r_{\rm out}} \rho_0 \left[1 + \left(\frac{r'}{r_c}\right)^2\right]^{-3\beta/2} r'^2 dr'$$

$$\Sigma(x,y) = \Sigma_0 \left(1 + \frac{x^2+y^2}{r_c^2}\right)^{-(3\beta-1)/2}$$

$$\Sigma_0 = \sqrt{\pi}\rho_0 r_c \frac{\Gamma\left(\frac{3\beta-1}{2}\right)}{\Gamma\left(\frac{3}{2}\beta\right)}$$

- In the weak field Newtonian limit we have (JWM, 2005, 2006):

$$a(r) = -\frac{G(r)M(r)}{r^2}$$

$$\mathcal{G}(r) \equiv \frac{G(r)}{G_N} = 1 + \sqrt{\frac{M_0}{M(r)}}\left\{1 - \exp\left(-\frac{r}{r_0}\right)\left(1 + \frac{r}{r_0}\right)\right\} \qquad \mathcal{G}_\infty = 1 + \sqrt{\frac{M_0}{M}}$$

- $G_N = 6.6742 \times 10^{-11}$ $\mathrm{m^3/kg\,s^2}$ is the ordinary (terrestial) Newtonian gravitational constant measured experimentally[2],
- $M(r)$ is the total (ordinary) mass enclosed in a sphere or radius, r. This may include all of the visible (X-ray) ICM gas and all of the galactic (baryonic) matter, but none of the non-baryonic dark matter.
- M_0 is the MOG mass scale (usually measured in units of $[M_\odot]$),
- r_0 is the MOG range parameter (usually measured in units of [kpc]).

- In the weak field Newtonian limit we have (JWM, 2005, 2006):

$$a(r) = -\frac{G(r)M(r)}{r^2}$$

$$\mathcal{G}(r) \equiv \frac{G(r)}{G_N} = 1 + \sqrt{\frac{M_0}{M(r)}}\left\{1 - \exp\left(-\frac{r}{r_0}\right)\left(1 + \frac{r}{r_0}\right)\right\}$$

$$\mathcal{G}_\infty = 1 + \sqrt{\frac{M_0}{M}}$$

- $G_N = 6.6742 \times 10^{-11}$ $\mathrm{m^3/kg\,s^2}$ is the ordinary (terrestial) Newtonian gravitational constant measured experimentally[2],
- $M(r)$ is the total (ordinary) mass enclosed in a sphere or radius, r. This may include all of the visible (X-ray) ICM gas and all of the galactic (baryonic) matter, but none of the non-baryonic dark matter.
- M_0 is the MOG mass scale (usually measured in units of $[M_\odot]$),
- r_0 is the MOG range parameter (usually measured in units of [kpc]).

• The goal of the strong and weak lensing survey of Bradac et al. (2006), Clowe et al. (2006) was to obtain a convergence κ-map by measuring the distortion images of background galaxies by the deflection of light as it passes the bullet cluster (lens). The distortions in image ellipticity are only measurable statistically with a large number of sources. The reduced shear g=γ/(1-κ) is measured where γ is the anisotropic stretching of the galaxy image, and the convergence κ is the shape-independent change in the size of the image. By recovering the κ-map from the measured reduced shear field, a measure of the local curvature is obtained. In GR and in MOG, the local curvature is related to the distribution of mass/energy.

$$\kappa(x,y) = \int \frac{4\pi G(r)}{c^2} \frac{D_\mathrm{l} D_\mathrm{ls}}{D_\mathrm{s}} \rho(x,y,z) dz \equiv \frac{\Sigma(x,y)}{\Sigma_c(r)}$$

$$\Sigma_c = \frac{c^2}{4\pi G_N} \frac{D_\mathrm{s}}{D_\mathrm{l} D_\mathrm{ls}} \approx 3.1 \times 10^9 \; M_\odot/\mathrm{kpc}^2$$

$$\kappa(x,y) = \int \frac{4\pi G(r)}{c^2} \frac{D_\mathrm{l} D_\mathrm{ls}}{D_\mathrm{s}} \rho(x,y,z) dz \equiv \frac{\bar{\Sigma}(x,y)}{\Sigma_c}$$

$$\bar{\Sigma}(x,y) = \int \mathcal{G}(r) \rho(x,y,z) dz$$

$$\frac{D_\mathrm{l} D_\mathrm{ls}}{D_\mathrm{s}} \approx 540 \; \mathrm{kpc}$$

$$\mathcal{G}(r) \equiv \frac{G(r)}{G_N} = 1 + \sqrt{\frac{M_0}{M(r)}} \left\{ 1 - \exp\left(-\frac{r}{r_0}\right) \left(1 + \frac{r}{r_0}\right) \right\}$$

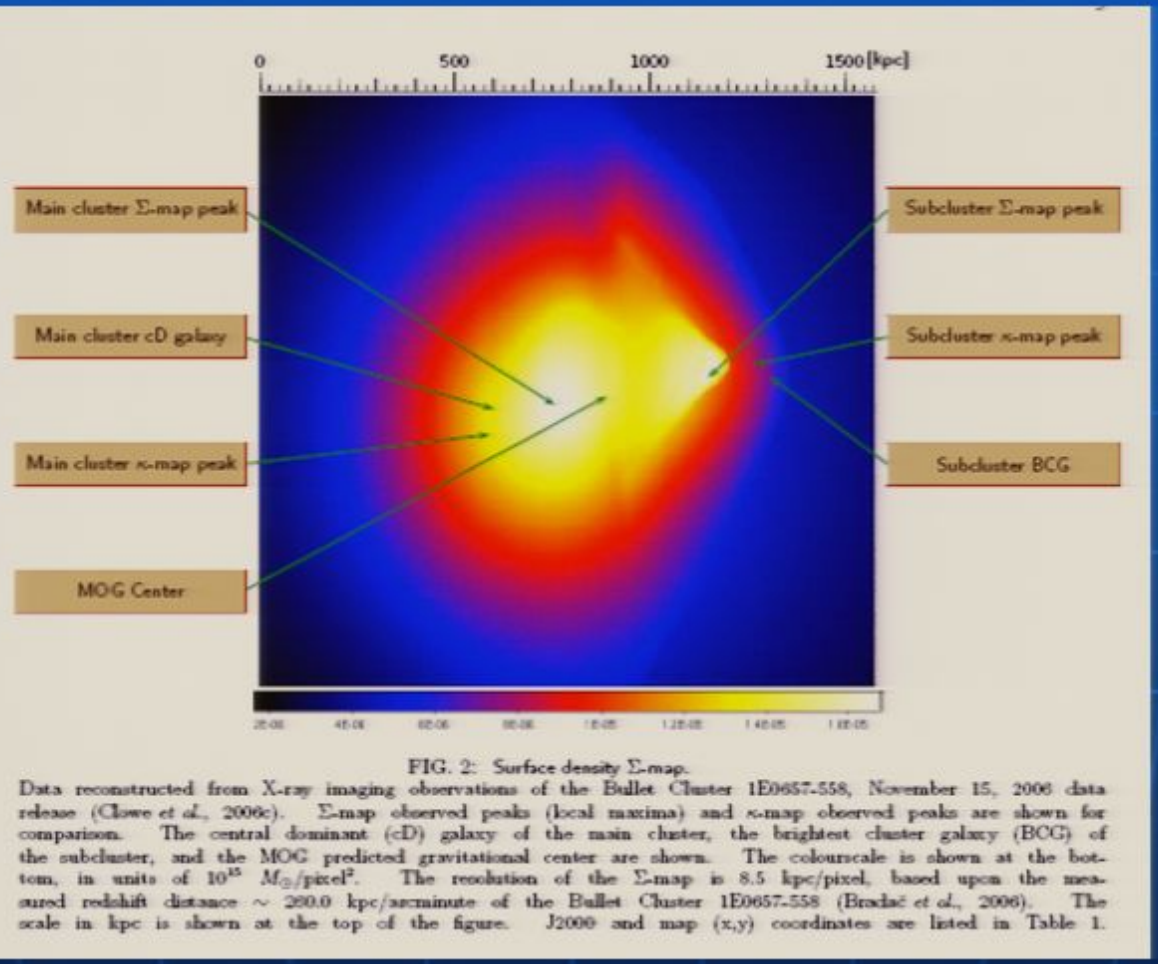

FIG. 2: Surface density Σ-map.
Data reconstructed from X-ray imaging observations of the Bullet Cluster 1E0657-558, November 15, 2006 data release (Clowe *et al.*, 2006c). Σ-map observed peaks (local maxima) and κ-map observed peaks are shown for comparison. The central dominant (cD) galaxy of the main cluster, the brightest cluster galaxy (BCG) of the subcluster, and the MOG predicted gravitational center are shown. The colourscale is shown at the bottom, in units of 10^{15} $M_\odot$/pixel^2. The resolution of the Σ-map is 8.5 kpc/pixel, based upon the measured redshift distance ~ 280.0 kpc/arcminute of the Bullet Cluster 1E0657-558 (Bradač *et al.*, 2006). The scale in kpc is shown at the top of the figure. J2000 and map (x,y) coordinates are listed in Table 1.

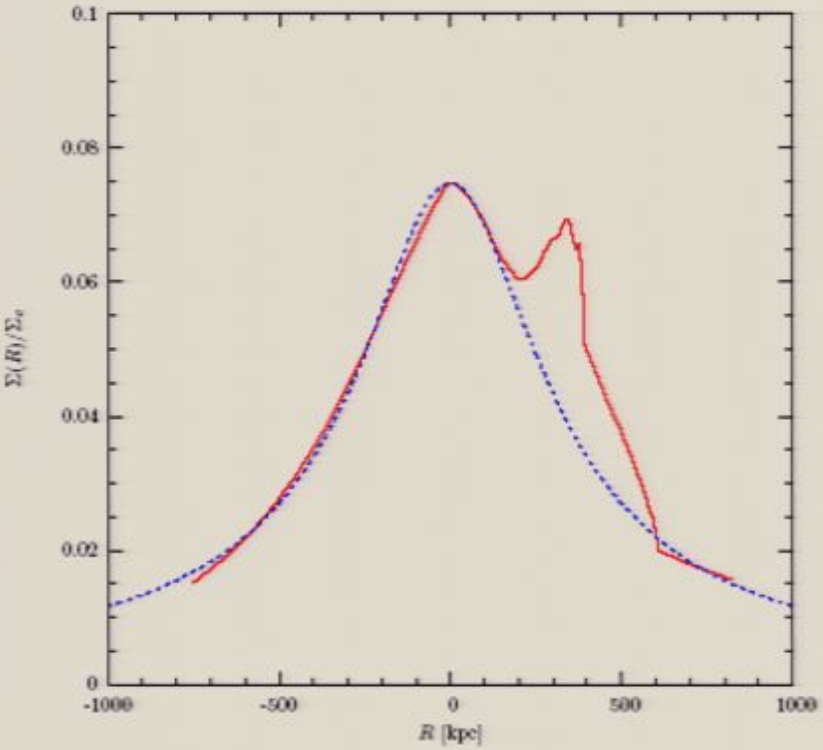

FIG. 3: King β-model fit to scaled Σ-map.
A cross-section of the scaled surface density Σ-map data reconstructed from X-ray imaging observations of the Bullet Cluster 1E0657-558, on a straight-line connecting the main X-ray cluster peak ($R \equiv 0$ kpc) to the main central dominant (cD) galaxy ($R \approx -150$ kpc). The Main cluster Σ-map data, taken from the November 15, 2006 data release (Clowe *et al.*, 2006c), is shown in solid red, and the surface density Σ-map according to the best-fit King β-model (neglecting the subcluster) of Equation (18) is shown in short-dashed blue. The unmodeled peak (at $R \sim 300$ kpc) is due to the subcluster. We used the Clowe *et al.* (2004) value for the Newtonian critical surface mass density (with vanishing shear), $\Sigma_c = 3.1 \times 10^9\ M_\odot/\mathrm{kpc}^2$. J2000 and map (x,y) coordinates are listed in Table 1. The best-fitting King β-model parameters are listed in Table 2.

$$\beta = 0.803 \pm 0.013,$$
$$r_c = 278.0 \pm 6.8\ \mathrm{kpc},$$

$$\rho_0 = \frac{\Sigma_0}{\sqrt{\pi} r_c} \frac{\Gamma\left(\frac{3}{2}\beta\right)}{\Gamma\left(\frac{3\beta-1}{2}\right)} = 3.34 \times 10^5\ M_\odot/\mathrm{kpc}^2$$

$$M_0 = 1.02 \times 10^{16}\ M_\odot$$

$$\mathcal{G}_\infty = 6.14$$

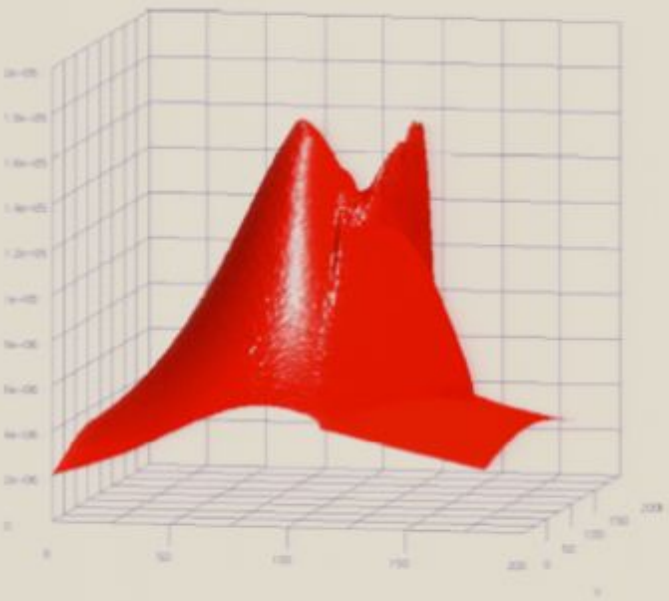

(a) Σ-map

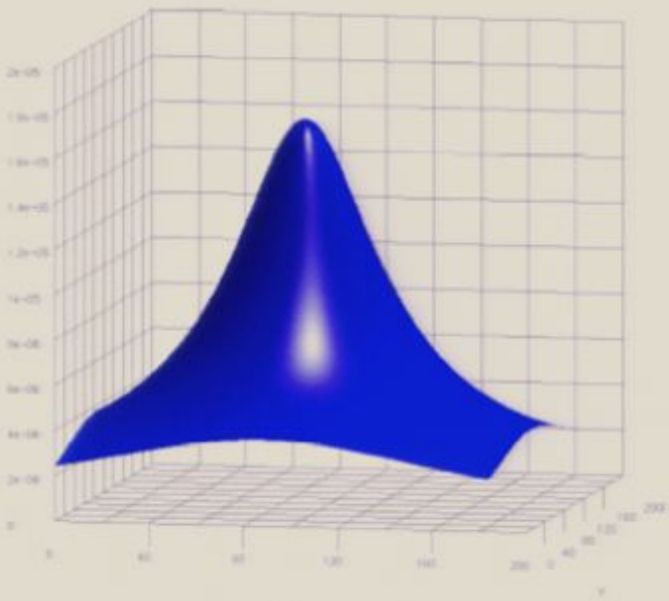

(b) King β-model

FIG. 4: Comparison of the Σ-map data and the best-fit King β-model. The surface density Σ-map data reconstructed from X-ray imaging observations of the Bullet Cluster 1E0657-558, November 15, 2006 data release (Clowe *et al.*, 2006c), is shown in red (a). The surface density Σ-map according to the best-fit King β-model (neglecting the subcluster) of Equation (18) is shown in blue (b). The best-fitting King β-model parameters are listed in Table 2.

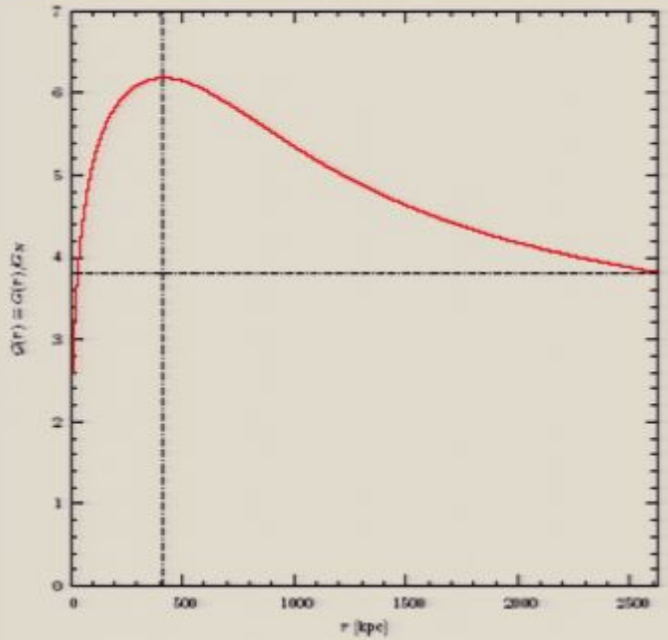

(a) Linear Scale, r-axis.

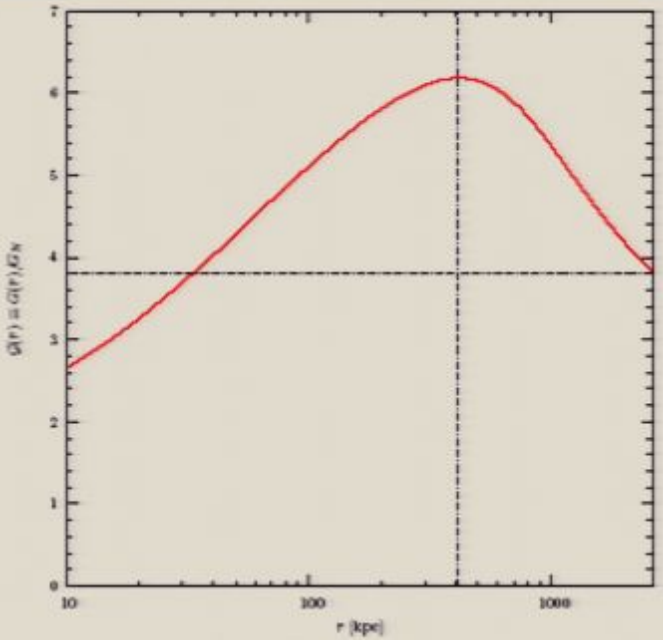

(b) Logarithmic Scale, r-axis.

FIG. 6: Plot of the dimensionless gravitational coupling, $\mathcal{G}(r) \equiv G(r)/G_N$, of Equation (1) vs. the distance, r, in kpc. Shown in linear scale for the r-axis, (a), and in logarithmic scale, (b). J2000 and map (x,y) coordinates of the MOG center ($R \equiv 0$ kpc) are listed in Table 1, and located with respect to the Σ-map and κ-map in Figures 2 and 11, respectively. The running gravitational coupling, $\mathcal{G}(r)$, shown here, corresponds to our best-fit to the κ-map, listed in Table 3.

One-dimensional cartoon sketch of MOG lensing prediction.

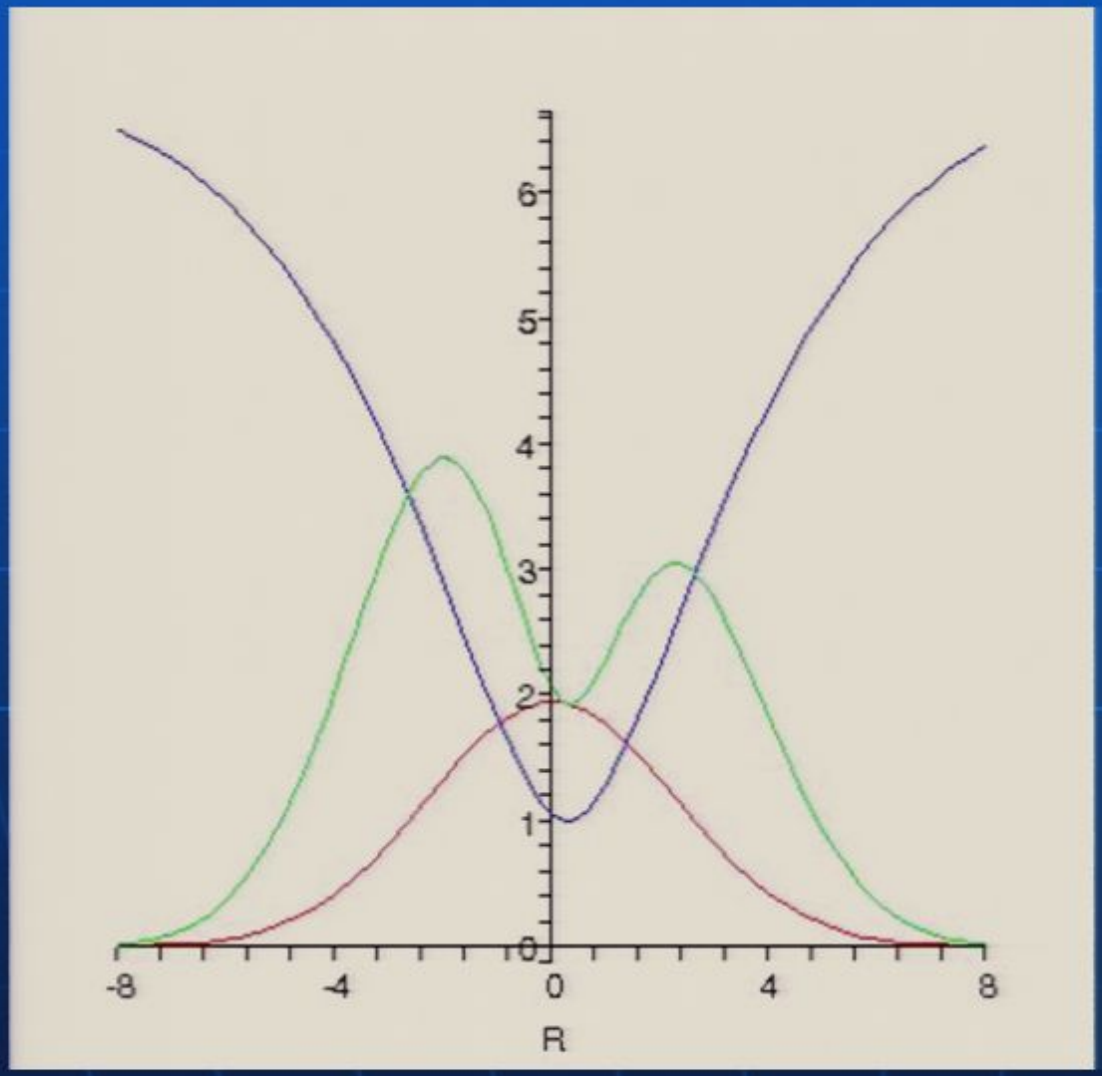

Red curve is X-ray gas surface density $\Sigma(R)$.

Blue curve is $G(R)/G_N$.

Green curve is predicted $\kappa(R)$ lensing.

One-dimensional cartoon sketch of MOG lensing prediction.

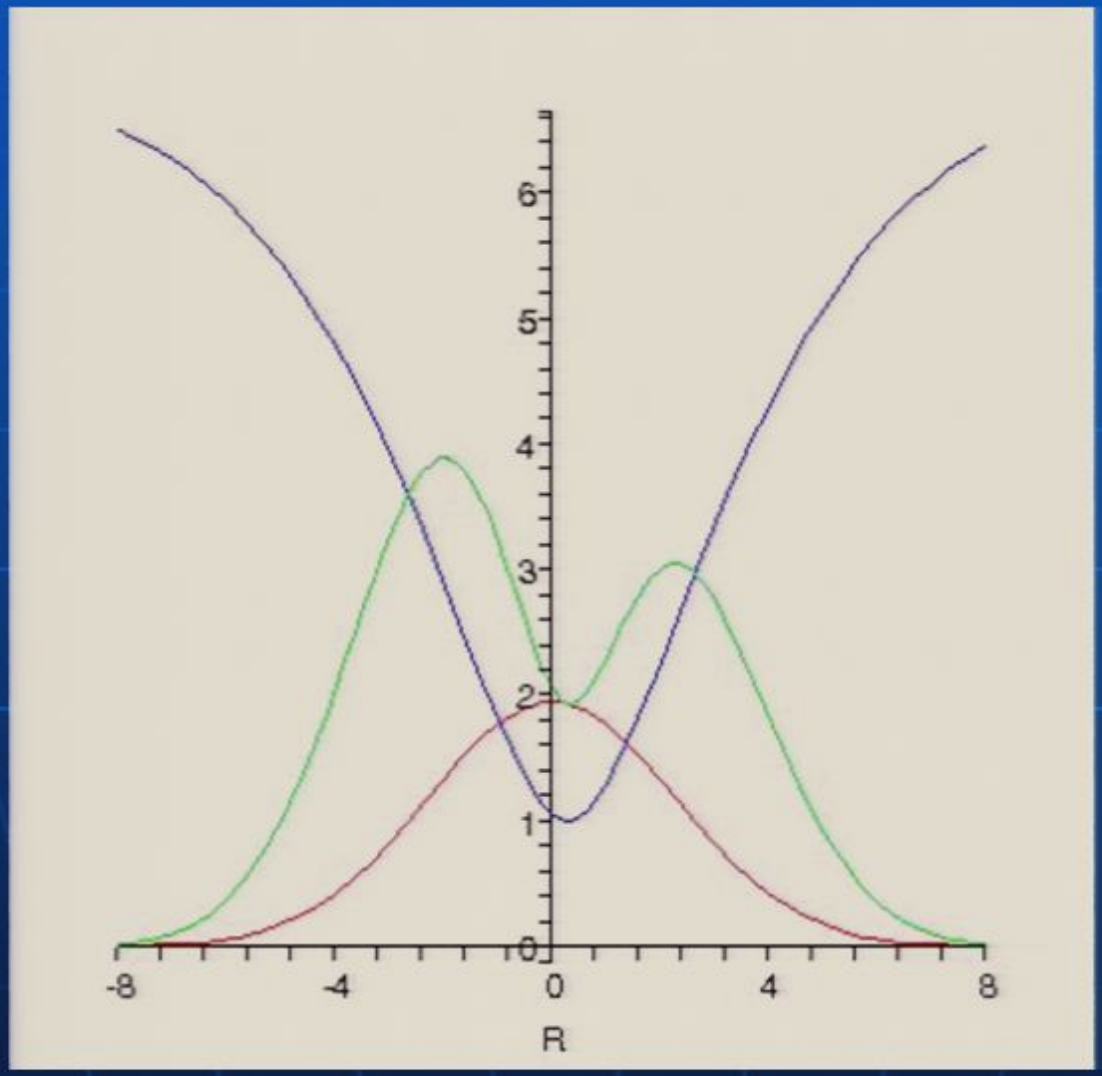

Red curve is X-ray gas surface density $\Sigma(R)$.

Blue curve is $G(R)/G_N$.

Green curve is predicted $\kappa(R)$ lensing.

- For a spherically system in hydrostatic equilibrium:

$$\frac{dP(r)}{dr} = -\rho(r)\frac{d\Phi(r)}{dr}$$

$$\sigma_r^2 = \frac{kT(r)}{\mu m_p}$$

$$\frac{d}{dr}\left(\frac{kT(r)}{\mu m_p}\rho(r)\right) = -\rho(r)\frac{d\Phi(r)}{dr}$$

$$\begin{aligned} a(r) &\equiv -\frac{d\Phi(r)}{dr} \\ &= \frac{kT(r)}{\mu m_p r}\left[\frac{d\ln(\rho(r))}{d\ln(r)} + \frac{d\ln(T(r))}{d\ln(r)}\right] \end{aligned}$$

$$M_{\rm MOG}(r) = \frac{3\beta kT}{\mu m_p G(r)}\left(\frac{r^3}{r^2 + r_c^2}\right)$$

- MOG *predicts the temperature T of the main cluster:*

Year	Source - Theory or Experiment	T (keV)	% error
2007	MOG Prediction	15.5 ± 3.9	
2002	accepted experimental value	$14.8^{+1.7}_{-1.2}$	4.5
1999	ASCA+ROSAT fit	$14.5^{+2.0}_{1.7}$	6.5
1998	ASCA fit	17.4 ± 2.5	12.3

TABLE 4: The MOG best-fit temperature is consistent with the experimental values for the main cluster isothermal temperature, the 1999 ASCA+ROSAT fit, and the 1998 ASCA fit (Markevitch *et al.*, 2002).

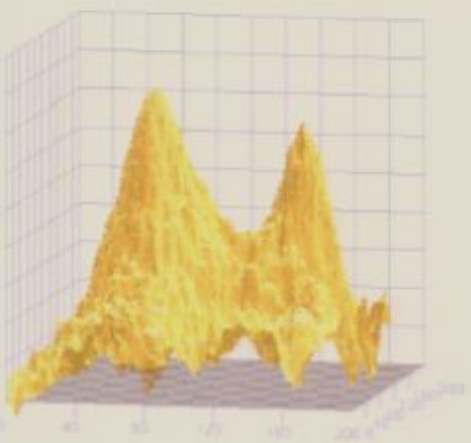

(a) 3D visualization of the κ-map November 15, 2006 data release (Clowe *et al.*, 2006c)

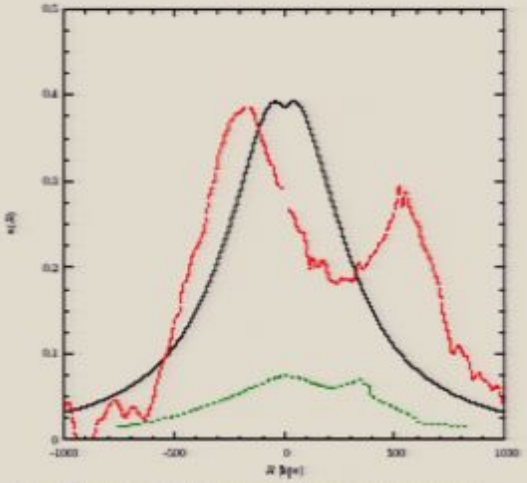

(b) 0^{th}-order approximation – neglecting the subcluster

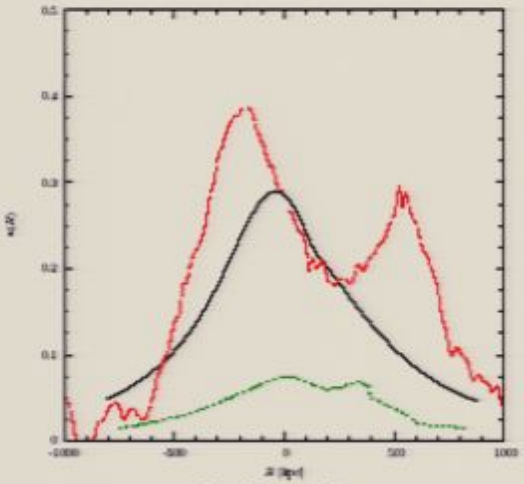

(c) Best-fit κ-model

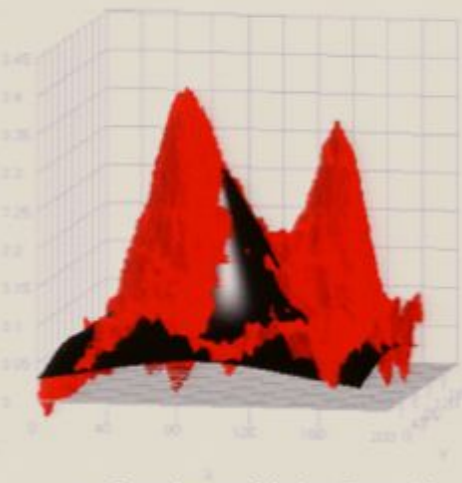

(d) 3D visualization of the best-fit κ-model

FIG. 12: The convergence κ-map November 15, 2006 data release (Clowe *et al.*, 2006c) and our κ-models. The best-fit MOG κ-model is shown in solid black in Figures 12b, 12c and 12d. The convergence κ-map November 15, 2006 data release (Clowe *et al.*, 2006c) is shown as Figure 12a and in red in Figures 12b, 12c and 12d. The scaled Σ-map, $\Sigma(x,y)/\Sigma_c$ data is shown in short-dashed green, also shown in Figure 3.

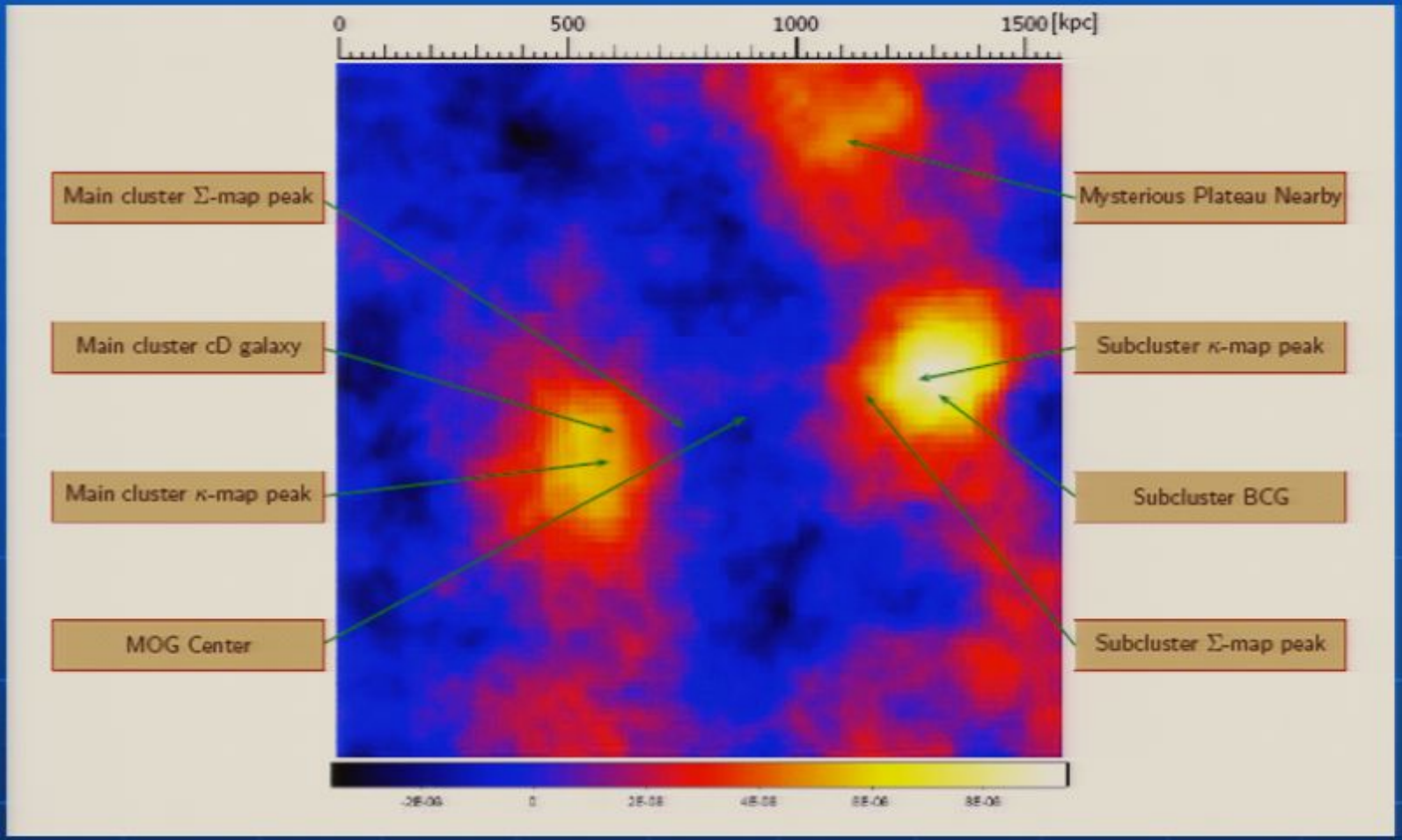

FIG. 13: The galaxy surface density Σ-map prediction.
The prediction of the Σ-map due to the galaxies as computed by the difference between the κ-map and our MOG κ-model, scaled as surface mass density according to Equation (64). Σ-map and κ-map observed peaks are shown for comparison. The central dominant (cD) galaxy of the main cluster, the brightest cluster galaxy (BCG) of the subcluster, and the MOG predicted gravitational center are shown. J2000 and map (x,y) coordinates are listed in Table 1. Component masses (integrated within a 100 kpc radius aperture) for the main and subcluster, the MOG center and the total predicted baryonic mass, $M_{\rm bary}$, for the Bullet Cluster 1E0657-558 are shown in Table 5.

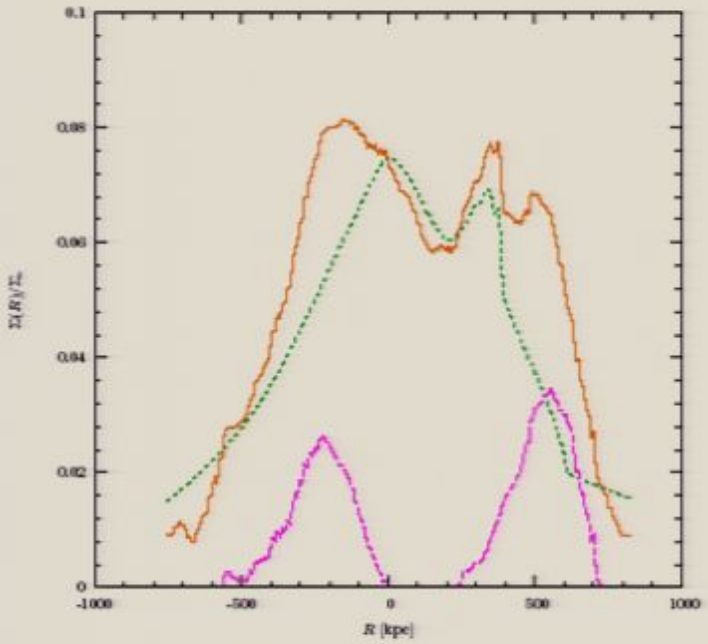

(a) Scaled surface density for the MOG predicted galaxies, $\Sigma_{\rm galax}/\Sigma_c$, and the MOG predicted visible baryons, $\Sigma_{\rm bary}/\Sigma_c$, compared to the ICM gas.

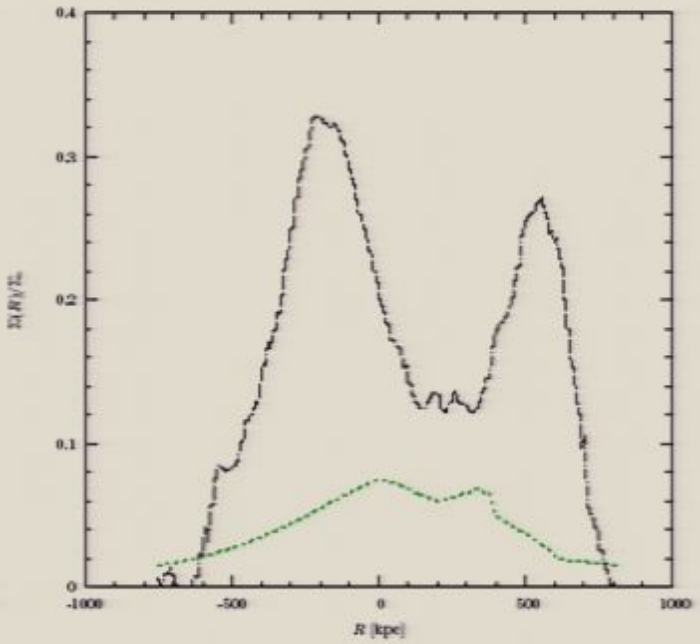

(b) Scaled surface density of dark matter, $\Sigma_{\rm DM}/\Sigma_c$, compared to ICM gas.

FIG. 14: Plot of the scaled surface density Σ/Σ_c along the line connecting the main cluster Σ-map peak with the main cD. In Figure 14a, the prediction of Equation (64) for the galaxies is shown in long-dashed magenta, and the prediction of Equation (66) for the visible baryonic mass is shown in solid brown. The calculation of Equation (67) for dark matter is shown in Figure 14b in dash-dot black. The ICM gas distribution inferred from the Σ-map data is shown in short-dashed green on each plot.

$$\Sigma_{\rm galax}(x,y) \approx \frac{\kappa(x,y)\Sigma_c - \bar{\Sigma}(x,y)}{\mathcal{G}(x,y)}$$

$$\Sigma_{\rm DM}(x,y) \approx \kappa(x,y)\Sigma_c - \Sigma(x,y)$$

$$M_{\rm DM} = \Sigma_c \int \kappa(x',y')dx'\,dy' - \int \Sigma(x',y')dx'\,dy'$$

• The mass ratios $M_{\_galax}/M_{gas}$ for the main and subcluster and central ICM are shown in Table 5. The result of $M_{\_galax}/M_{gas}$ ~ 0.4 % in the central ICM is due to the excellent fit in the MOG across the hundreds of kpc separating the main and the subcluster. The dark matter result of M_{gas}/M_{DM} ~ 45 % in the central ICM implies that the evolutionary dark matter scenario does not lead to a spatial dissociation between the dark matter and the ICM gas, which indicates that the merger is ongoing. In contrast, the MOG result shows a true dissociation between the galaxies and the ICM gas as required by the evolutionary scenario. The baryon to dark matter fraction over the full Σ-map is 32 %, which is significantly higher than the Λ-CDM cosmological baryon mass-fraction of 17 ± 1.9 % (Spergel et al. 2006).

Component	Main cluster	Subcluster	Central ICM	Total
M_{gas}	$7.0 \times 10^{12}\ M_\odot$	$5.8 \times 10^{12}\ M_\odot$	$6.3 \times 10^{12}\ M_\odot$	$2.2 \times 10^{14}\ M_\odot$
M_{galax}	$1.8 \times 10^{12}\ M_\odot$	$3.1 \times 10^{12}\ M_\odot$	$2.4 \times 10^{10}\ M_\odot$	$3.8 \times 10^{13}\ M_\odot$
M_{bary}	$8.8 \times 10^{12}\ M_\odot$	$9.0 \times 10^{12}\ M_\odot$	$4.9 \times 10^{12}\ M_\odot$	$2.6 \times 10^{14}\ M_\odot$
M_{DM}	$2.1 \times 10^{13}\ M_\odot$	$1.7 \times 10^{13}\ M_\odot$	$1.4 \times 10^{13}\ M_\odot$	$6.8 \times 10^{14}\ M_\odot$
M_{galax}/M_{gas}	26%	53%	0.4%	17%
M_{gas}/M_{DM}	33%	34%	45%	32%

TABLE 5: Summary of component mass predictions. Component masses (integrated within a 100 kpc radius aperture) for the main and subcluster and the MOG center. The total predicted mass for the Bullet Cluster 1E0657-558 is integrated over the full Σ-map.

• Cosmological model solution for $G(t)/G_N$ versus t obtained from STVG field equation for G(t). Here, $G(t)/G_N = 1$ at $t=t^*$ where $t^*=t_{BBN}$ (time of Big Bang nucleosynthesis) and $G(t)/G_N \sim 7$ for $t \sim t_r$ before recombination.

$$\mathcal{G}(t) = 1 + \bar{\omega}\left[1 - \exp\left(-\frac{(t-t^*)^2}{t_c^2}\right)\right]$$

$$\mathcal{G}(t) = G(t)/G_N$$

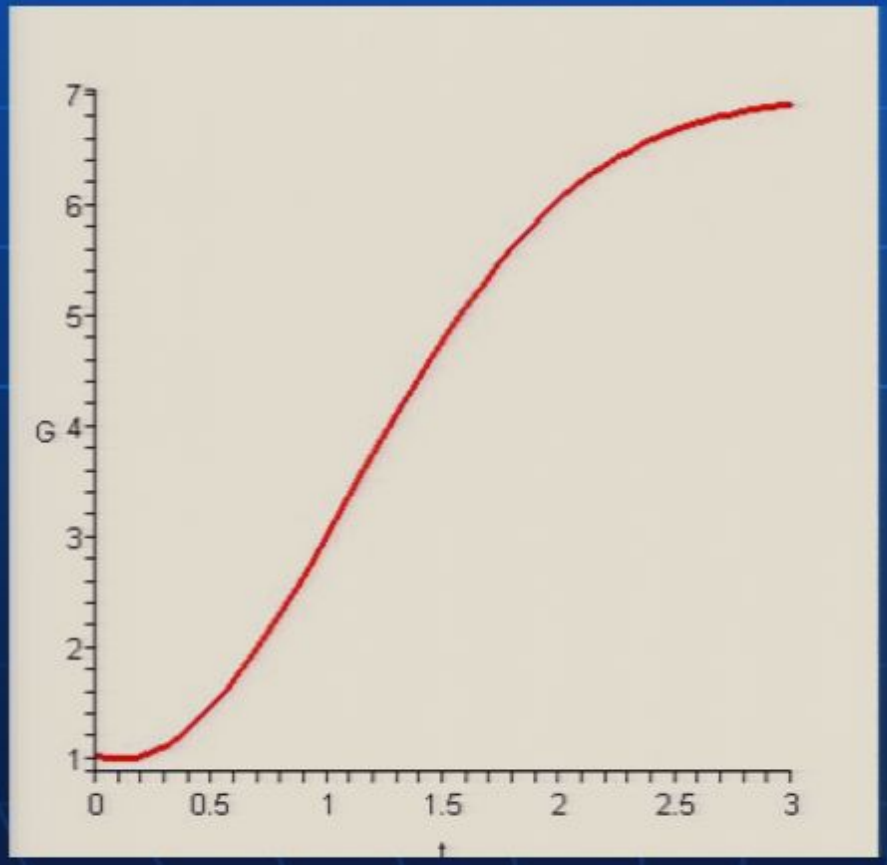

$$G(t*) = G_N$$

$$G(t_r) \sim 7G_N$$

6. MOG Cosmology

- We adopt a FLRW background spacetime:

$$ds^2 = dt^2 - a^2(t)\left(\frac{dr^2}{1-kr^2} + r^2 d\Omega^2\right)$$

$$\phi_0 \equiv \phi \neq 0,\ \phi_i = 0 \text{ and } B_{\mu\nu} = 0$$

- The modified Friedmann equations are

$$\frac{\dot{a}^2}{a^2} + \frac{k}{a^2} = \frac{8\pi G\rho}{3} + \Lambda_G,$$
$$\frac{\ddot{a}}{a} = -\frac{4\pi G}{3}(\rho + 3p) + \Lambda_G$$

$$H^2 = \frac{8\pi G_{\rm eff}\rho_m}{3} + \Lambda_G$$

$$\Lambda_G = H\frac{\dot{G}}{G} > 0$$

$$G_{\rm eff}(t_r) = G_N(1+Z) = \text{const.}$$

$$\Omega_m + \Omega_G = 1$$

$$\Omega_m = \frac{8\pi G_{\rm eff}\rho_m}{3H^2},\quad \Omega_G = \frac{\Lambda_G}{H^2}.$$

$$\Omega_m \sim \Omega_{b\rm eff}$$

• Cosmological model solution for $G(t)/G_N$ versus t obtained from STVG field equation for G(t). Here, $G(t)/G_N = 1$ at $t=t^*$ where $t^*=t_{BBN}$ (time of Big Bang nucleosynthesis) and $G(t)/G_N \sim 7$ for $t \sim t_r$ before recombination.

$$\mathcal{G}(t) = 1 + \bar{\omega}\left[1 - \exp\left(-\frac{(t-t^*)^2}{t_c^2}\right)\right]$$

$$\mathcal{G}(t) = G(t)/G_N$$

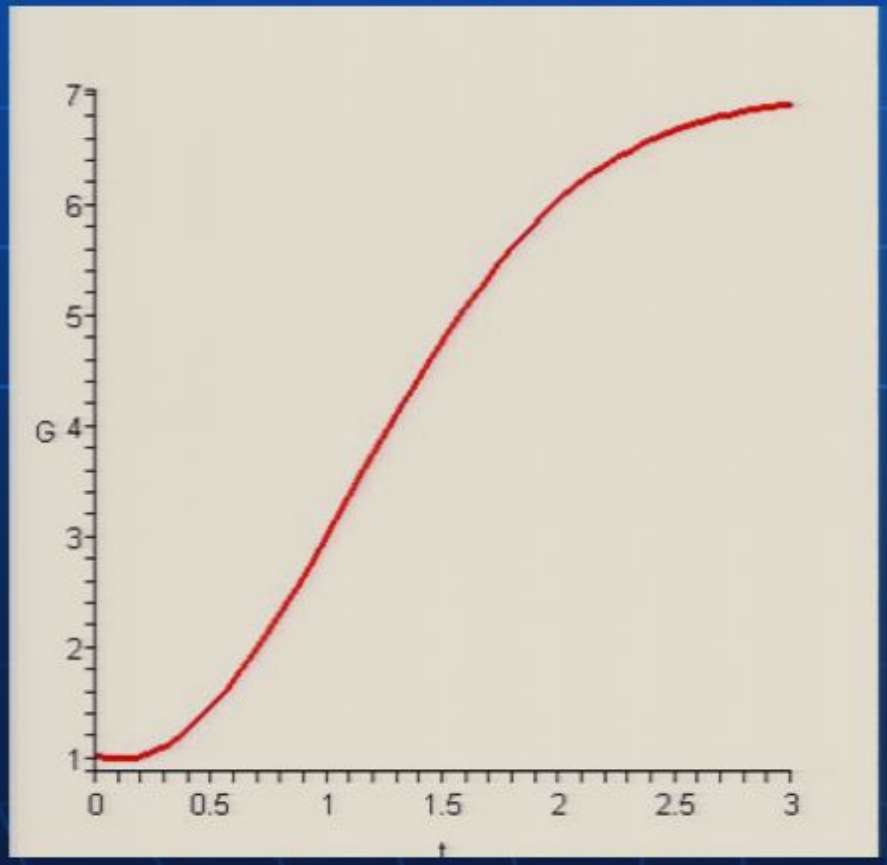

$$G(t*) = G_N$$

$$G(t_r) \sim 7G_N$$

• The correlation function for the temperature differences across the sky for a given angle theta takes the form:

$$C(\theta) = \frac{1}{4\pi}\sum_{l=2}^{\infty}(2l+1)C_l P_l(\cos\theta),$$

$\Omega_{bN} \sim 0.04, \quad \Omega_{b\text{eff}} \sim 0.3, \quad \Omega_G \sim 0.7, \quad \xi \sim 0.6,$

$r_h = 0.03, \quad r_p = 0.01 \quad l_f \sim 1580, \quad l_s \sim 1100.$

where $\Omega_{bN} = 8\pi G_N \rho_b / 3H^2.$

$$\Omega_m = \frac{8\pi G_{\text{eff}}\rho_m}{3H^2}, \quad \Omega_G = \frac{\Lambda_G}{H^2}.$$

$\Omega_m \sim \Omega_{b\text{eff}},$

$$\Omega_{b\text{eff}} = \frac{8\pi G_{\text{eff}}\rho_b}{3H^2}.$$

$$\xi \equiv \frac{1}{3c_s^2} - 1 = \frac{3}{4}\left(\frac{\rho_b}{\rho_\gamma}\right)$$

• The correlation function for the temperature differences across the sky for a given angle theta takes the form:

$$C(\theta) = \frac{1}{4\pi}\sum_{l=2}^{\infty}(2l+1)C_l P_l(\cos\theta),$$

• I use a modified form of the analytic calculation of C_l given by Mukhanov (2006) to obtain a fit to the acoustical peaks in the CMB for l > 100 < 1200. Assuming that the baryon fluid dominates, the adopted density parameters are

$$\Omega_{bN} \sim 0.04, \quad \Omega_{b\mathrm{eff}} \sim 0.3, \quad \Omega_G \sim 0.7, \quad \xi \sim 0.6,$$

$$r_h = 0.03, \quad r_p = 0.01 \quad l_f \sim 1580, \quad l_s \sim 1100.$$

where $\Omega_{bN} = 8\pi G_N \rho_b / 3H^2.$

$$\Omega_m = \frac{8\pi G_{\mathrm{eff}}\rho_m}{3H^2}, \quad \Omega_G = \frac{\Lambda_G}{H^2},$$

$$\Omega_m \sim \Omega_{b\mathrm{eff}},$$

$$\Omega_{b\mathrm{eff}} = \frac{8\pi G_{\mathrm{eff}}\rho_b}{3H^2},$$

$$\xi \equiv \frac{1}{3c_s^2} - 1 = \frac{3}{4}\left(\frac{\rho_b}{\rho_\gamma}\right)$$

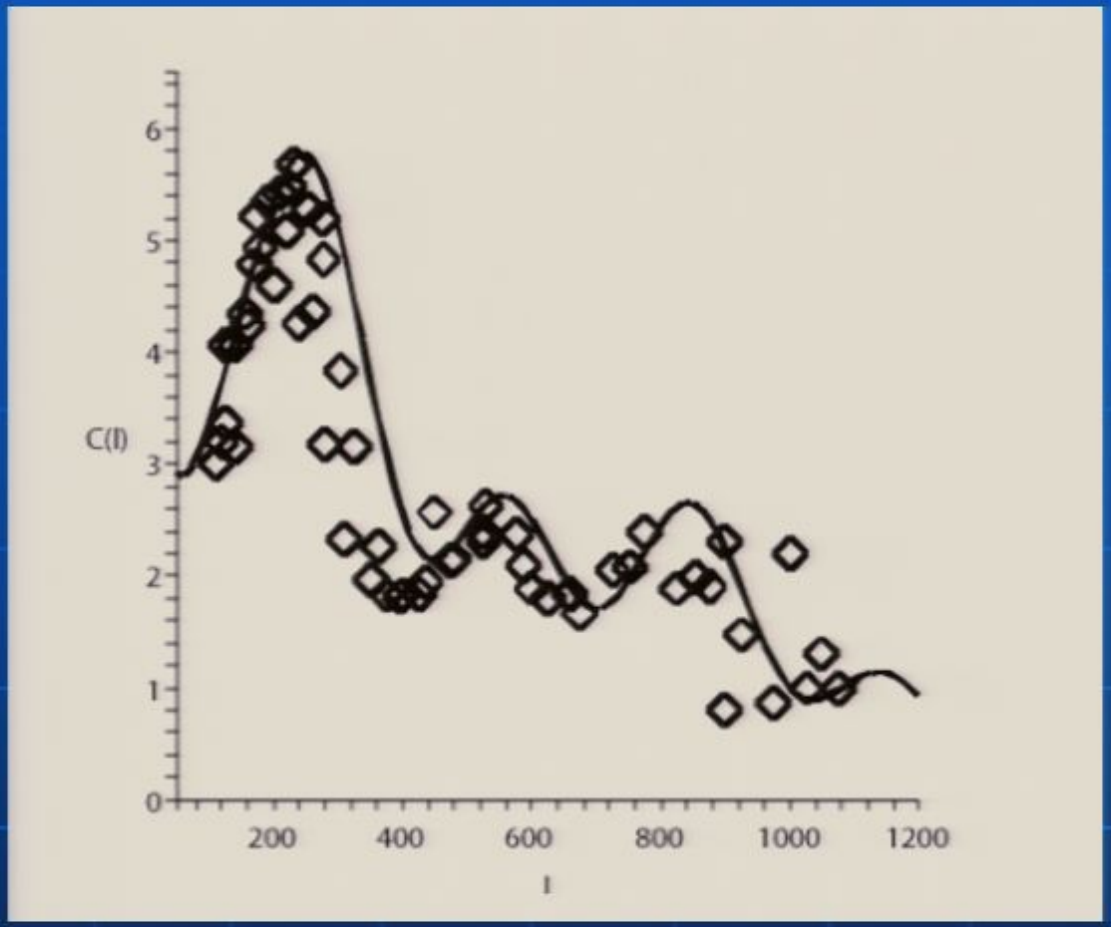

Fig. 1. The solid line shows the result of the calculation of the power spectrum acoustical oscillations: $C(l)$, and the $\diamond s$ correspond to the WMAP, Archeops and Boomerang data in units $\mu K^2 \times 10^{-3}$ as presented in Refs. 27-30.

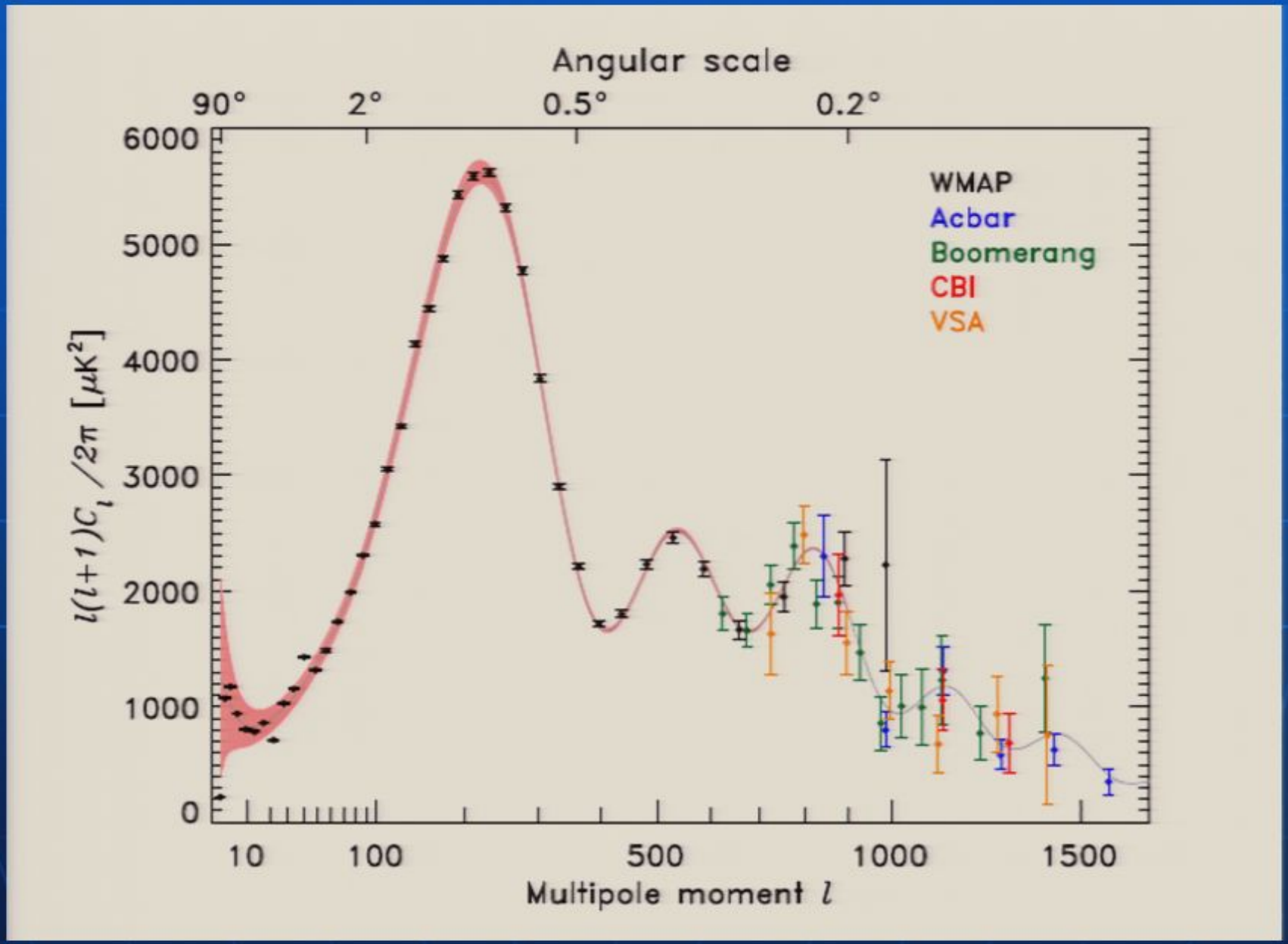
Angular scale
90°
2°
0.5°
0.2°
6000
5000
4000
3000
2000
1000
0
$l(l+1)C_l/2\pi$ [μK^2]
WMAP
Acbar
Boomerang
CBI
VSA
10
100
500
1000
1500
Multipole moment l

• The role played by CDM in the standard ΛCDM model is replaced in MOG by the significant deepening of the gravitational wells before recombination with $G_{\rm eff} \sim 7G_N$, which traps the baryons. This reduces the baryon dissipation due to the photon coupling pressure (Silk dampening) and the third and higher peaks in the acoustical oscillation spectrum are not suppressed due to finite thickness and baryon drag effects. The effective baryon density $\Omega_{b\rm eff} = (1+Z)\Omega_{bN} \sim 7\Omega_{bN} \sim 0.3$ dominates before recombination and we fit the acoustical spectrum without a collisionless dark matter component.

• The accelerated expansion of the universe follows from our MOG. The generalized Friedmann equations take the approximate form for a spatially flat universe

$$H^2 = \frac{8\pi G_{\rm eff}\rho_m}{3} + \Lambda_G, \qquad \Omega_m + \Omega_G = 1, \qquad \Lambda_G = H\frac{\dot{G}}{G} > 0, \qquad \dot{\Lambda}_G \sim 0.$$

$$\Omega_m = \frac{8\pi G_{\rm eff}\rho_m}{3H^2}, \quad \Omega_G = \frac{\Lambda_G}{H^2},$$

Consider the MOG effective cosmological constant (Einstein's cosmological constant $\Lambda = 0$):

$$\Lambda_G = H\frac{\dot{G}}{G} > 0$$

From MOG fits to WMAP3 power spectrum:

$$\Omega_G = \frac{\Lambda_G}{H^2}. \sim 0.7$$

Substituting $H_0 \sim 7\text{x}10^{-11}\ \text{yr}^{-1}$ we obtain for cosmological scales $z > 0.05$:

$$|\dot{G}/G| \sim \ 10^{-11}\ \text{yr}^{-1}$$

The experimental bound in the local solar system is

$$|\dot{G}/G| \sim \ 10^{-12}\ \text{yr}^{-1}.$$

- The gravitational instability governing over-densities $\delta = \delta\rho/\rho$ reads schematically:

$$\ddot{\delta} + [\text{Pressure} - \text{Gravity}]\delta = 0$$

- If pressure is low δ grows exponentially, while if pressure is high δ oscillates with time. The effective increase in the gravitational constant $G_{\text{eff}} \sim 7G_N$ produces growth at earlier times before recombination copying the effects of cold dark matter. Thus, the observed power spectrum can be predicted by MOG without cold dark matter, avoiding the non-observed oscillating behavior predicted by the baryon fluid with only 4% baryons.
- We need to do N-body simulations with MOG without dark matter to investigate whether we can reproduce the galaxy and void structure observed in large-scale surveys.

- The gravitational instability governing over-densities $\delta = \delta\rho/\rho$ reads schematically:

$$\ddot{\delta} + [\text{Pressure} - \text{Gravity}]\delta = 0$$

- If pressure is low δ grows exponentially, while if pressure is high δ oscillates with time. The effective increase in the gravitational constant $G_{\text{eff}} \sim 7G_N$ produces growth at earlier times before recombination copying the effects of cold dark matter. Thus, the observed power spectrum can be predicted by MOG without cold dark matter, avoiding the non-observed oscillating behavior predicted by the baryon fluid with only 4% baryons.
- We need to do N-body simulations with MOG without dark matter to investigate whether we can reproduce the galaxy and void structure observed in large-scale surveys.

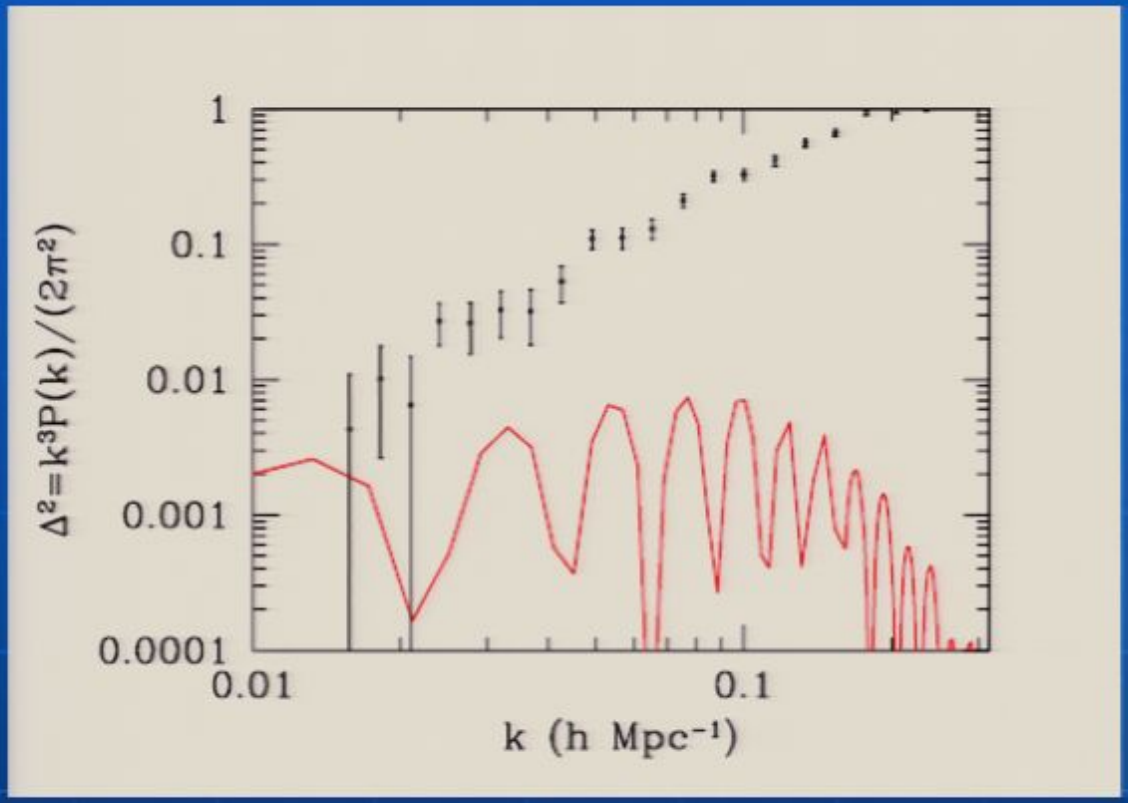

From Scott Dodelson and Michele Liguori, Phys.Rev.Lett. 97 (2006) 231301, astro-ph/0608602.

FIG. 1: Power spectrum of matter fluctuations in a theory without dark matter as compared to observations of the galaxy power spectrum. The observed spectrum [14] does not have the pronounced wiggles predicted by a baryon-only model, but it also has significantly higher power than does the model. In fact Δ^2, which is a dimensionless measure of the clumping, never rises above one in a baryon-only model, so we would not expect to see any large structures (clusters, galaxies, people, etc.) in the universe in such a model.

7. Conclusions

• A stable and self-consistent modified gravity (MOG) is constructed from a pseudo-Riemannian geometry and a massive skew field obtained from the curl of a massive vector field (phion field) (STVG). The static spherically symmetric solution of the field equations yields a modified Newtonian acceleration law with a distance scale dependence. The gravitational "constant" G, the effective mass and the coupling strength of the skew field run with distance scale r according to an infra-red RG flow scenario, based on an "asymptotically" free quantum gravity. This can be described by an effective classical STVG action.

7. Conclusions

• A stable and self-consistent modified gravity (MOG) is constructed from a pseudo-Riemannian geometry and a massive skew field obtained from the curl of a massive vector field (phion field) (STVG). The static spherically symmetric solution of the field equations yields a modified Newtonian acceleration law with a distance scale dependence. The gravitational "constant" G, the effective mass and the coupling strength of the skew field run with distance scale r according to an infra-red RG flow scenario, based on an "asymptotically" free quantum gravity. This can be described by an effective classical STVG action.

• A fit to 101 galaxy rotations curves is obtained and mass profiles of x-ray galaxy clusters are also successfully fitted for those clusters that are isothermal.

• A possible explanation of the Pioneer 10-11 anomalous acceleration is obtained from the MOG with predictions for the onset of the anomalous acceleration at Saturn's orbit and for the periods of the outer planets.

• A fit to the bullet cluster 1E0657-56 data can be achieved with the (renormalized) "running" of the gravitational "constant' G without dark matter. The lensing of galaxies and clusters can be explained without dark matter.

• The CMB power spectrum acoustical peaks data including the third peak can be fitted with the density parameters:

$$\Omega_m = \frac{8\pi G_{\text{eff}}\rho_m}{3H^2}, \quad \Omega_G = \frac{\Lambda_G}{H^2}$$

• Preliminary work shows that the power spectrum for growth of fluctuations and the formation of galaxies and clusters can be incorporated in MOG without dark matter.

• A fit to the bullet cluster 1E0657-56 data can be achieved with the (renormalized) "running" of the gravitational "constant' G without dark matter. The lensing of galaxies and clusters can be explained without dark matter.

Without Non-Baryonic Dark Matter, Mon. Not. Roy. Astron. Soc. 367 (2006) 527, astro-ph/0507222

• J. R. Brownstein and J. W Moffat, Gravitational Solution to the Pioneer 10/11 Anomaly, Class. Quant. Grav. 23, 3427 (2006), gr-qc/0511026

• J. W. Moffat, Time Delay Predictions in a Modified Gravity Theory, Class. Quant. Grav. 23, 6767 (2006), gr-qc/0605141

•J. W. Moffat, Gravitational Theory, Galaxy Rotation Curves and Cosmology without Dark Matter, JCAP 0505 (2005) 003, astro-ph/0412195

• J. R. Brownstein and J. W. Moffat, The Bullet Cluster 1E0657-558 Evidence Shows Modified Gravity Without Dark Matter, astro-ph/0702146

• J. W. Moffat, Int. J. Mod. Phys. D (to be published), gr-qc/0608074, astro-ph/0702416

MOG Bibliography

- J. W. Moffat, Scalar-Tensor-Vector Gravity Theory, JCAP 0603 (2006) 004, gr-qc/0506021
- J. R. Brownstein and J. W Moffat, Galaxy Rotation Curves without Non-Baryonic Dark Matter, Astrophys. J. 636 (2006) 721, astro-ph/0506370
- J. R. Brownstein and J. W Moffat, Galaxy Cluster Masses Without Non-Baryonic Dark Matter, Mon. Not. Roy. Astron. Soc. 367 (2006) 527, astro-ph/0507222
- J. R. Brownstein and J. W Moffat, Gravitational Solution to the Pioneer 10/11 Anomaly, Class. Quant. Grav. 23, 3427 (2006), gr-qc/0511026
- J. W. Moffat, Time Delay Predictions in a Modified Gravity Theory, Class. Quant. Grav. 23, 6767 (2006), gr-qc/0605141
- J. W. Moffat, Gravitational Theory, Galaxy Rotation Curves and Cosmology without Dark Matter, JCAP 0505 (2005) 003, astro-ph/0412195
- J. R. Brownstein and J. W. Moffat, The Bullet Cluster 1E0657-558 Evidence Shows Modified Gravity Without Dark Matter, astro-ph/0702146
- J. W. Moffat, Int. J. Mod. Phys. D (to be published), gr-qc/0608074, astro-ph/0702416